Prospects of very long baseline neutrino oscillation experiments with the KEK-JAERI high intensity proton accelerator

Mayumi Aoki,[1,*] K. Hagiwara,[1] Y. Hayato,[2,†] T. Kobayashi,[2,‡] T. Nakaya,[3,§] K. Nishikawa,[3,‖] and N. Okamura[4,¶]
[1]*Theory Group, KEK, Tsukuba, Ibaraki 305-0801, Japan*
[2]*Institute of Particle and Nuclear Studies, High Energy Accelerator Research Org. (KEK), Tsukuba, Ibaraki 305-0801, Japan*
[3]*Department of Physics, Kyoto University, Kyoto 606-8502, Japan*
[4]*IPPAP, Physics Department, Virginia Tech., Blacksburg, Virginia 24061*
(Received 27 December 2001; revised manuscript received 19 February 2003; published 20 May 2003)

We study the physics potential of very long baseline neutrino-oscillation experiments with a high intensity proton accelerator which will be completed by the year 2007 in Tokai-village, as a joint project of KEK and JAERI (Japan Atomic Energy Research Institute). The 50 GeV proton synchrotron at J-PARC (Japan Proton Accelerator Research Complex) will deliver neutrino beams in the range of a few GeV with an intensity about two orders of magnitude higher than the present KEK beam for the K2K experiment. As a sequel to the proposed J-PARC–to–Super-Kamiokande experiment, we study the impact of experiments with a 100 kton-level detector and a baseline length of a few-thousand km. The pulsed narrow-band ν_μ beams allow us to measure the $\nu_\mu \to \nu_e$ transition probability and the ν_μ survival probability through counting experiments at a large water-Čerenkov detector. We study the sensitivity of such experiments to the neutrino mass hierarchy, the mass-squared differences, the three angles, and one CP phase of the three-generation lepton-flavor-mixing matrix. We find that experiments at a distance between 1000 and 2000 km can determine the sign of the larger mass-squared difference $(m_3^2 - m_1^2)$ if the mixing between ν_e and ν_3 (the heaviest-or-lightest neutrino) is not too small: $4|U_{e3}|^2(1-|U_{e3}|^2) \gtrsim 0.03$. The CP phase can be constrained if the $|U_{e3}|$ element is sufficiently large: $4|U_{e3}|^2(1-|U_{e3}|^2) \gtrsim 0.06$, and if the smaller mass-squared difference $(m_2^2 - m_1^2)$ and the U_{e2} element are in the preferred range of the large-mixing-angle solution of the solar-neutrino deficit. The magnitude $|m_3^2 - m_1^2|$ and the matrix element $U_{\mu 3}$ can be precisely measured, but we find little sensitivity to $m_2^2 - m_1^2$ and the matrix element U_{e2}.

DOI: 10.1103/PhysRevD.67.093004 PACS number(s): 14.60.Lm, 14.60.Pq

I. INTRODUCTION

Many neutrino experiments [1–10] strongly suggest that there are flavor mixings in the lepton sector, and that neutrinos are massive. According to the atmospheric-neutrino observations [1], the lepton-flavor-mixing matrix [the Maki-Nakagawa-Sakata (MNS) matrix [11]] has a large mixing angle. Especially, the Super-Kamiokande (SK) Collaboration [2] reported that ν_μ oscillates into the other species with maximal mixing. The K2K [3] experiment, the current long-baseline (LBL) neutrino oscillation experiment from KEK to SK with $L = 250$ km and $\langle E_\nu \rangle = 1.3$ GeV, obtained results which are consistent with the neutrino oscillation in the atmospheric-neutrino anomaly with $\delta m^2 \sim 3 \times 10^{-3}$ and $\sin^2 2\theta \sim 1$. The two reactor neutrino experiments CHOOZ [4] and Palo Verde [5] reported that no oscillation is found from $\overline{\nu}_e$, and they exclude significant mixing between $\overline{\nu}_e$ and the other neutrinos. An important conclusion from these observations is that the atmospheric neutrino oscillation cannot be due to ν_μ-ν_e oscillation. Recently, the SK Collaboration showed evidence that ν_μ oscillates into an active neutrino rather than sterile neutrinos [6]. According to the results of solar-neutrino observations [7], the ν_e flux from the Sun is less than that of the prediction of the standard solar model [8] and the reduction factor depends on neutrino energies. The most convincing explanation for this deficit is the ν_e oscillation to the other neutrinos. Four possible scenarios of the solar-neutrino oscillation have been identified: the Mikheyev-Smirnov-Wolfenstein (MSW) [12,13] large-mixing-angle (LMA) solution, the MSW small-mixing-angle (SMA) solution, the vacuum oscillation (VO) solution [14], and the MSW low-δm^2 (LOW) solution. Recently, the SK Collaboration reported the energy spectrum and the day-night asymmetry data and showed that the LMA solution is more favorable than the other scenarios [9]. The SNO experiment [10], which observes the solar neutrino flux with heavy water, showed conclusively, when combined with the SK flux data, that ν_e oscillates into the other active neutrinos.[1] A consistent picture of three-neutrino oscillations with two large mixing angles and two hierarchically different mass-squared differences emerges from those observations, with the exception of the LSND experiment [15] which may indicate the existence of the fourth and nonstandard (sterile) neutrino.

*Email address: mayumi.aoki@kek.jp
†Email address: hayato@neutrino.kek.jp
‡Email address: takashi.kobayashi@kek.jp
§Email address: nakaya@scphys.kyoto-u.ac.jp
‖Email address: nishikaw@neutrino.kek.jp
¶Email address: nokamura@vt.edu

[1]While this manuscript was being prepared, the KamLAND Collaboration reported that only the LMA solutions are consistent with their observation of reactor antineutrinos [51].

Several LBL neutrino oscillation experiments [16–19] and a short-baseline experiment [20] have been proposed to confirm the results of these experiments and to measure the neutrino oscillation parameters more precisely. The MINOS experiments [16], from Fermilab to the Soudan mine, with a baseline length of $L=730$ km and $\langle E_\nu\rangle=3.5$ GeV, will start producing data in 2005. The observation of the survival probability $P_{\nu_\mu\to\nu_\mu}$ will allow us to measure the larger mass-squared difference and the mixing angle with about 10% accuracy. Two LBL experiments ICARUS [17] and OPERA [18], from CERN to Gran Sasso with a baseline length of $L=730$ km and at higher energies with $\langle E_\nu\rangle\sim 20$ GeV have been proposed, and they may begin operation in 2005. The CERN experiments expect to observe the $\nu_\mu\to\nu_\tau$ appearance. The physics discover potential of these LBL experiments has been studied extensively [21].

In Japan, as a sequel to the K2K experiment, a new LBL neutrino oscillation experiment between the Japan Proton Accelerator Research Complex (J-PARC) [22] and SK has been proposed [19]. The facility, J-PARC, has a 50 GeV proton synchrotron (PS), which will be completed by the year 2007 in Tokai-village as a joint project of KEK and JAERI (Japan Atomic Energy Research Institute). The J-PARC PS can deliver high intensity neutrino beams in the ~ 1 GeV range, whose intensity is two-orders-of-magnitude higher than that of the KEK 12 GeV proton synchrotron beam for the K2K experiment. The J-PARC–to–SK experiment with $L=295$ km and $\langle E_\nu\rangle=1.3$ GeV will measure the larger mass-squared difference with 3% accuracy and the mixing angle at about 1% accuracy.

All these experiments use conventional neutrino beams, which are made from decaying pions and kaons that are produced by high-energy proton beams. The possibility of a neutrino factory [23] has been discussed as the next generation of LBL neutrino-oscillation experiments [24]. Here the neutrino beam is delivered from decaying muons in a muon-storage ring, where the stored muon energy may be in the range of several 10 GeV. A neutrino factory can deliver very high intensity neutrino beams that are consist of the same amount of ν_μ and $\bar{\nu}_e$ ($\bar{\nu}_\mu$ and ν_e from μ^+) with precisely known spectra. The possibility of constructing a neutrino factory in the JAERI site by upgrading the J-PARC PS is now being extensively studied [25].

In this paper we examine the alternative possibility of using conventional neutrino beams from the J-PARC for very-long-baseline (VLBL) neutrino oscillation experiments, whose baseline length exceeds a thousand km [26]. A possible 100 kton detector in Beijing [27] can be a target at about $L=2100$ km away. The physics capability of such experiments should be seriously studied because a neutrino factory may turn out to be too difficult or too expensive to realize in the near future. In order to take full advantage of conventional ν beams, we examine the case of using pulsed narrow-band ν_μ beams (NBBs) and as a target we consider a large water-Čerenkov detector similar to SK which is capable of measuring the ν_μ-to-ν_e transition probability and the ν_μ survival probability. We study the sensitivity of such experiments to the signs and magnitudes of the two mass-squared differences, the three angles, and one CP phase of the three-flavor MNS matrix.

This article is organized as follows. In Sec. II, we fix our notation and review the present status of the neutrino-oscillation experiments in the three-neutrino model. In Sec. III, we study the properties of the narrow-band neutrino beams that can be delivered by the J-PARC 50 GeV PS. In Sec. IV, we study the signals, backgrounds, and systematic errors of the VLBL experiments and present our findings for the prospects of experiments at baseline lengths of 2100 and 1200 km. All our main findings are summarized compactly in Sec. V.

II. NEUTRINO OSCILLATION IN THE THREE-NEUTRINO MODEL

In this section, we give the definition and useful parametrization of the 3×3 Maki-Nakagawa-Sakata (MNS) lepton-flavor-mixing matrix [11], and give constraints on its matrix elements and the neutrino mass-squared differences.

A. The MNS matrix

The MNS matrix is defined analogously to the CKM matrix [28] through the charged current (CC) weak interactions, where the charged-current can be expressed as

$$J^\mu_{\rm CC}=(\bar{d},\bar{s},\bar{b})V^\dagger_{\rm CKM}\gamma^\mu(1-\gamma_5)(u,c,t)^T + (\bar{e},\bar{\mu},\bar{\tau})\gamma^\mu(1-\gamma_5)V_{\rm MNS}(\nu_1,\nu_2,\nu_3)^T. \quad (2.1)$$

Here $\nu_i(i=1,2,3)$ denotes the neutrino mass-eigenstates. The flavor eigenstates of the neutrinos are then expressed as

$$\nu_\alpha=\sum_{i=1}^{3}(V_{\rm MNS})_{\alpha i}\nu_i, \quad (2.2)$$

where $\alpha=e,\mu,\tau$ are the lepton-flavor indices.

The 3×3 MNS matrix has three mixing angles and three phases in general. We adopt the following parametrization [29]:

$$V_{\rm MNS}=\begin{pmatrix} U_{e1} & U_{e2} & U_{e3}\\ U_{\mu 1} & U_{\mu 2} & U_{\mu 3}\\ U_{\tau 1} & U_{\tau 2} & U_{\tau 3}\end{pmatrix}\begin{pmatrix} 1 & 0 & 0\\ 0 & e^{i\varphi_2} & 0\\ 0 & 0 & e^{i\varphi_3}\end{pmatrix}\equiv U\mathcal{P}, \quad (2.3)$$

where $\mathcal{P}$ is the diagonal phase matrix with two Majorana phases φ_2 and φ_3. The matrix U, which has three mixing angles and one phase, can be parametrized in the same way as the CKM matrix. Because the present neutrino oscillation experiments constrain directly the elements U_{e2}, U_{e3}, and $U_{\mu 3}$, we find it most convenient to adopt the parametrization [29] where these three matrix elements in the upper-right corner of the U matrix are the independent parameters. Without losing generality, we can take U_{e2} and $U_{\mu 3}$ to be real and non-negative. By allowing U_{e3} to have the complex phase

$$U_{e2},U_{\mu 3}\geqslant 0, \quad U_{e3}\equiv|U_{e3}|e^{-i\delta_{\rm MNS}} \ (0\leqslant\delta_{\rm MNS}<2\pi), \quad (2.4)$$

the four independent parameters are U_{e2}, $U_{\mu 3}$, $|U_{e3}|$, and $\delta_{\rm MNS}$. All the other matrix elements of the U are then determined by the unitary conditions

$$U_{e1}=\sqrt{1-|U_{e3}|^2-|U_{e2}|^2}, \quad U_{\tau 3}=\sqrt{1-|U_{e3}|^2-|U_{\mu 3}|^2}, \tag{2.5a}$$

$$U_{\mu 1}=-\frac{U_{e2}U_{\tau 3}+U_{\mu 3}U_{e1}U_{e3}^*}{1-|U_{e3}|^2}, \tag{2.5b}$$

$$U_{\mu 2}=\frac{U_{e1}U_{\tau 3}-U_{\mu 3}U_{e2}U_{e3}^*}{1-|U_{e3}|^2}, \tag{2.5c}$$

$$U_{\tau 1}=\frac{U_{e2}U_{\mu 3}-U_{\tau 3}U_{e1}U_{e3}^*}{1-|U_{e3}|^2}, \tag{2.5d}$$

$$U_{\tau 2}=-\frac{U_{\mu 3}U_{e1}+U_{e2}U_{\tau 3}U_{e3}^*}{1-|U_{e3}|^2}. \tag{2.5e}$$

In this phase convention, U_{e1}, U_{e2}, $U_{\mu 3}$, and $U_{\tau 3}$ are all real and non-negative numbers, and the other five elements are complex numbers.

The Jarlskog parameter [30] of the MNS matrix is defined as

$$\begin{aligned} J_{\rm MNS} &\equiv {\rm Im}(V_{\alpha i}V_{\beta i}^*V_{\beta j}V_{\alpha j}^*) \\ &= {\rm Im}(U_{\alpha i}U_{\beta i}^*U_{\beta j}U_{\alpha j}^*) \\ &= -\frac{U_{e1}U_{e2}U_{\mu 3}U_{\tau 3}}{1-|U_{e3}|^2}{\rm Im}(U_{e3}), \end{aligned} \tag{2.6}$$

where $(\alpha,\beta)=(e,\mu),(\mu,\tau),(\tau,e)$ and $(i,j)=(1,2),(2,3),(3,1)$. The last expression above is obtained in our phase convention. The two Majorana phases φ_2 and φ_3 do not contribute to the Jarlskog parameter.

B. Constraints on the MNS matrix and the mass-squared differences

The probability of finding the flavor-eigenstate β from the original flavor-eigenstate α at the baseline length L in the vacuum is given by

$$\begin{aligned} P_{\nu_\alpha\to\nu_\beta} &= \left|\sum_{j=1}^{3}(V_{\rm MNS})_{\beta j}\exp\left(-i\frac{m_j^2}{2E_\nu}L\right)(V_{\rm MNS})_{j\alpha}\right|^2 \\ &= |U_{\beta 1}U_{\alpha 1}^{ast}+U_{\beta 2}e^{-i\Delta_{12}}U_{\alpha 2}^*+U_{\beta 3}e^{-i\Delta_{13}}U_{\alpha 3}^*|^2 \\ &= \delta_{\alpha\beta}-4\,{\rm Re}\Big\{U_{\alpha 1}U_{\beta 1}^*U_{\beta 2}U_{\alpha 2}^*\sin^2\frac{\Delta_{12}}{2} \\ &\quad +U_{\alpha 2}U_{\beta 2}^*U_{\beta 3}U_{\alpha 3}^*\sin^2\frac{\Delta_{23}}{2} \\ &\quad +U_{\alpha 3}U_{\beta 3}^*U_{\beta 1}U_{\alpha 1}^*\sin^2\frac{\Delta_{31}}{2}\Big\} \\ &\quad +2\,{\rm Im}[U_{\alpha 1}U_{\beta 1}^*U_{\beta 2}U_{\alpha 2}^*] \\ &\quad \times[\sin\Delta_{12}+\sin\Delta_{23}+\sin\Delta_{31}], \end{aligned} \tag{2.7}$$

where Δ_{ij} is

$$\Delta_{ij}\equiv\frac{\delta m_{ij}^2}{2E_\nu}L\simeq 2.534\frac{\delta m_{ij}^2({\rm eV}^2)}{E_\nu({\rm GeV})}L({\rm km}), \tag{2.8}$$

with the neutrino energy E_ν and the mass-squared differences $\delta m_{ij}^2=m_j^2-m_i^2$. In particular, the survival probability in the vacuum is

$$\begin{aligned} P_{\nu_\alpha\to\nu_\alpha} &= 1-4\Big\{|U_{\alpha 1}U_{\alpha 2}|^2\sin^2\frac{\Delta_{12}}{2}+|U_{\alpha 2}U_{\alpha 3}|^2\sin^2\frac{\Delta_{23}}{2} \\ &\quad +|U_{\alpha 3}U_{\alpha 1}|^2\sin^2\frac{\Delta_{31}}{2}\Big\}. \end{aligned} \tag{2.9}$$

The oscillation probabilities of antineutrinos in the vacuum are obtained from those of neutrinos simply by reversing the sign of the Jarlskog parameter:

$$P_{\bar\nu_\alpha\to\bar\nu_\alpha}=P_{\nu_\alpha\to\nu_\alpha}, \tag{2.10a}$$

$$P_{\bar\nu_\alpha\to\bar\nu_\beta}=P_{\nu_\alpha\to\nu_\beta}(J_{\rm MNS}\to -J_{\rm MNS}). \tag{2.10b}$$

The following approximations for the oscillation probabilities are useful in our study. When $|\Delta_{12}|\ll|\Delta_{13}|\sim 1$, the oscillation probabilities can be expressed as

$$\begin{aligned} P_{\nu_\alpha\to\nu_\beta} &= \delta_{\alpha\beta}-4\,{\rm Re}\{U_{\alpha 3}U_{\beta 3}^*U_{\beta 1}U_{\alpha 1}^*+U_{\alpha 2}U_{\beta 2}^*U_{\beta 3}U_{\alpha 3}^*\} \\ &\quad \times\sin^2\frac{\Delta_{13}}{2}+\Big\{2\,{\rm Re}(U_{\alpha 2}U_{\beta 2}^*U_{\beta 3}U_{\alpha 3}^*)\sin\Delta_{13} \\ &\quad \pm 4J_{\rm MNS}\sin^2\frac{\Delta_{13}}{2}\Big\}\Delta_{12}-\{{\rm Re}(U_{\alpha 1}U_{\beta 1}^*U_{\beta 2}U_{\alpha 2}^* \\ &\quad +U_{\alpha 2}U_{\beta 2}^*U_{\beta 3}U_{\alpha 3}^*\cos\Delta_{13})\mp J_{\rm MNS}\sin\Delta_{13}\} \\ &\quad \times\Delta_{12}^2+\mathcal{O}(\Delta_{12}^3). \end{aligned} \tag{2.11}$$

When $1\ll|\Delta_{12}|\sim|\Delta_{13}|$, we may take into account finite resolution of Δ_{ij} ($\Delta_{ij}\to\Delta_{ij}\pm\delta\Delta_{ij}$), and find

$$P_{\nu_\alpha\to\nu_\beta}\to\frac{1}{2\,\delta\Delta_{ij}}\int_{\Delta_{ij}-\delta\Delta_{ij}}^{\Delta_{ij}+\delta\Delta_{ij}}d\Delta_{ij}P_{\nu_\alpha\to\nu_\beta}(\Delta_{ij})=\delta_{\alpha\beta}-2\,\mathrm{Re}\{U_{\alpha1}U_{\beta1}^*U_{\beta2}U_{\alpha2}^*+U_{\alpha2}U_{\beta2}^*U_{\beta3}U_{\alpha3}^*+U_{\alpha3}U_{\beta3}^*U_{\beta1}U_{\alpha1}^*\}$$
$$+2\,\mathrm{Re}\left\{U_{\alpha1}U_{\beta1}^*U_{\beta2}U_{\alpha2}^*\cos\Delta_{12}\frac{\sin\delta\Delta_{12}}{\delta\Delta_{12}}+U_{\alpha2}U_{\beta2}^*U_{\beta3}U_{\alpha3}^*\cos\Delta_{23}\frac{\sin\delta\Delta_{23}}{\delta\Delta_{23}}\right.$$
$$\left.+U_{\alpha3}U_{\beta3}^*U_{\beta1}U_{\alpha1}^*\cos\Delta_{31}\frac{\sin\delta\Delta_{31}}{\delta\Delta_{31}}\right\}\pm2J_{\mathrm{MNS}}\left\{\sin\Delta_{12}\frac{\sin\delta\Delta_{12}}{\delta\Delta_{12}}+\sin\Delta_{23}\frac{\sin\delta\Delta_{23}}{\delta\Delta_{23}}+\sin\Delta_{31}\frac{\sin\delta\Delta_{31}}{\delta\Delta_{31}}\right\}. \tag{2.12}$$

In LBL experiments the uncertainty in E_ν, δE_ν, dictates $\delta\Delta_{ij}$,

$$\delta\Delta_{ij}\simeq-\Delta_{ij}\frac{\delta E_\nu}{E_\nu}, \tag{2.13}$$

and the following two cases are relevant. When

$$|\delta\Delta_{12}|\simeq\left|\Delta_{12}\frac{\delta E_\nu}{E_\nu}\right|\ll1\ll\left|\Delta_{13}\frac{\delta E_\nu}{E_\nu}\right|\simeq|\delta\Delta_{13}|\simeq|\delta\Delta_{23}|, \tag{2.14}$$

Eq. (2.12) can be expressed as

$$P_{\nu_\alpha\to\nu_\beta}\to\delta_{\alpha\beta}-2\,\mathrm{Re}\{U_{\alpha1}U_{\beta1}^*U_{\beta2}U_{\alpha2}^*+U_{\alpha2}U_{\beta2}^*U_{\beta3}U_{\alpha3}^*+U_{\alpha3}U_{\beta3}^*U_{\beta1}U_{\alpha1}^*\}$$
$$+2\,\mathrm{Re}\{U_{\alpha1}U_{\beta1}^*U_{\beta2}U_{\alpha2}^*\cos\Delta_{12}\}\pm2J_{\mathrm{MNS}}\{\sin\Delta_{12}\}+\mathcal{O}\left[\left(\Delta_{12}\frac{\delta E_\nu}{E_\nu}\right)^2\right]+\mathcal{O}\left[\left(\Delta_{13}\frac{\delta E_\nu}{E_\nu}\right)^{-1}\right]. \tag{2.15}$$

On the other hand, when

$$1\ll\left|\Delta_{12}\frac{\delta E_\nu}{E_\nu}\right|\ll\left|\Delta_{13}\frac{\delta E_\nu}{E_\nu}\right| \tag{2.16}$$

Eq. (2.12) simplifies to

$$P_{\nu_\alpha\to\nu_\beta}\to\delta_{\alpha\beta}-2\,\mathrm{Re}\{U_{\alpha1}U_{\beta1}^*U_{\beta2}U_{\alpha2}^*+U_{\alpha2}U_{\beta2}^*U_{\beta3}U_{\alpha3}^*+U_{\alpha3}U_{\beta3}^*U_{\beta1}U_{\alpha1}^{ast}\}+\mathcal{O}\left[\left(\Delta_{12}\frac{\delta E_\nu}{E_\nu}\right)^{-1}\right]+\mathcal{O}\left[\left(\Delta_{13}\frac{\delta E_\nu}{E_\nu}\right)^{-1}\right]. \tag{2.17}$$

Note that in Eqs. (2.11), (2.12), and (2.15), $\pm J_{\mathrm{MNS}}$ stands for $\mathrm{Im}[U_{\alpha1}U_{\beta1}^*U_{\beta2}U_{\alpha2}^*]$; see Eq. (2.6).

All the above formulas remain valid for the neutrino oscillation probabilities in the matter, by replacing the mass-squared differences and the MNS matrix elements with the effective ones in the matter,

$$\Delta_{ij}\to\tilde{\Delta}_{ij},\quad U_{\alpha i}\to\tilde{U}_{\alpha i},\quad J_{\mathrm{MNS}}\to\tilde{J}_{\mathrm{MNS}}, \tag{2.18}$$

as long as the matter density remains the same along the baseline. The definitions of the effective parameters $\tilde{\Delta}_{ij}$ and $\tilde{U}_{\alpha i}$ are given in Sec. II D, and $\tilde{J}_{\mathrm{MNS}}$ is obtained from Eq. (2.6) by replacing all $U_{\alpha i}$'s by $\tilde{U}_{\alpha i}$'s.

In the following, we summarize the constraints on the neutrino mass-squared differences and the MNS matrix elements from the recent neutrino-oscillation experiments; the atmospheric-neutrino anomaly [1,2], the CHOOZ reactor experiment [4], and the solar-neutrino deficit observations [7,9,10].

1. Atmospheric-neutrino anomaly

A recent analysis of the atmospheric-neutrino data from the Super-Kamiokande (SK) experiment [2] finds

$$0.88<\sin^2 2\,\theta_{\mathrm{ATM}}<1.0, \tag{2.19a}$$

$$1.6\times10^{-3}<\delta m^2_{\mathrm{ATM}}(\mathrm{eV}^2)<4.0\times10^{-3}, \tag{2.19b}$$

from the $\nu_\mu\to\nu_\mu$ survival probability in the two-flavor oscillation model

$$P_{\nu_\mu\to\nu_\mu}=1-\sin^2 2\,\theta_{\mathrm{ATM}}\sin^2\left(\frac{\delta m^2_{\mathrm{ATM}}}{4E_\nu}L\right). \tag{2.20}$$

The baseline of this observation is less than about 10^4 km for the Earth diameter, and the typical neutrino energy is one to a few GeV. The survival probability Eq. (2.9) may then be expanded as

$$P_{\nu_\mu\to\nu_\mu}=1-4|U_{\mu3}|^2(1-|U_{\mu3}|^2)\sin^2\frac{\Delta_{13}}{2}+2|U_{\mu2}|^2|U_{mu3}|^2\Delta_{12}\sin\Delta_{13}+\mathcal{O}(\Delta_{12}^2). \tag{2.21}$$

When $|\Delta_{12}|\ll1$, we may neglect terms of order Δ_{12} and obtain the following identification:

$$4|U_{\mu3}|^2(1-|U_{\mu3}|^2)=\sin^2 2\,\theta_{\mathrm{ATM}}, \tag{2.22a}$$

$$|\delta m^2_{13}|=\delta m^2_{\mathrm{ATM}}. \tag{2.22b}$$

The independent parameter $U_{\mu3}$ ($\geqslant0$ in our convention) is then

$$U^2_{\mu 3} = \sin^2\theta_{\rm ATM}. \tag{2.23}$$

Note the twofold uncertainty in $\sin^2\theta_{\rm ATM}$ when $\sin^2 2\theta_{\rm ATM} < 1$.

The magnitude of the neglected terms in the above approximation is largest when the large-mixing-angle solution of the solar-neutrino deficit is taken. For $\delta m^2_{\rm SOL} = 10^{-4}$ eV^2, $E_\nu = 1$ GeV, and $L = 10^4$ km, we have $|\Delta_{12}| \simeq \delta m^2_{\rm SOL}(L/2E_\nu) \sim 1$, and more careful analyses in the three-neutrino model are required to constrain the model parameters. The results of such analyses [31] show that the identifications Eq. (2.22) remain valid approximately even for the large-mixing-angle solution.

2. Reactor neutrino experiments

The CHOOZ experiment [4] measured the survival probability of $\overline{\nu}_e$

$$P_{\overline{\nu}_e \to \overline{\nu}_e} = 1 - \sin^2 2\theta_{\rm RCT} \sin^2\left(\frac{\delta m^2_{\rm RCT}}{4E_\nu} L\right) \tag{2.24}$$

and it was found that

$$\sin^2 2\theta_{\rm RCT} < \begin{cases} 0.10 & \text{for} \quad \delta m^2_{\rm RCT} > 3.5\times 10^{-3}\ \text{eV}^2, \\ 0.18 & \text{for} \quad \delta m^2_{\rm RCT} > 2.0\times 10^{-3}\ \text{eV}^2, \\ 0.52 & \text{for} \quad \delta m^2_{\rm RCT} > 1.0\times 10^{-3}\ \text{eV}^2. \end{cases} \tag{2.25}$$

The baseline length of this experiment is about 1 km and the typical antineutrino energy is 1 MeV. For those L and E_ν, the Earth matter effects are negligible, and $|\Delta_{12}| = \delta m^2_{\rm SOL}(L/2E_\nu)$ can be safely neglected even for the large-mixing-angle solution. The survival probability of the three-neutrino model is then approximated by

$$P_{\overline{\nu}_e \to \overline{\nu}_e} = 1 - 4|U_{e3}|^2(1-|U_{e3}|^2)\sin^2\frac{\Delta_{13}}{2} + \mathcal{O}(\Delta_{12}) \tag{2.26}$$

and we obtain the identifications

$$4|U_{e3}|^2(1-|U_{e3}|^2) = \sin^2 2\theta_{\rm RCT}, \tag{2.27a}$$

$$|\delta m^2_{13}| = \delta m^2_{\rm RCT}. \tag{2.27b}$$

With the above identifications, we find that the element $|U_{e3}|$ Eq. (2.27a) is constrained by Eq. (2.25) in the region of $|\delta m^2_{13}|$ allowed by the atmospheric-neutrino oscillation data through Eqs. (2.19b) and (2.22b). The independent parameter U_{e3} is now constrained by Eq. (2.25) through the identification

$$|U_{e3}| = \sqrt{1-\sqrt{1-\sin^2 2\theta_{\rm RCT}}}/\sqrt{2}. \tag{2.28}$$

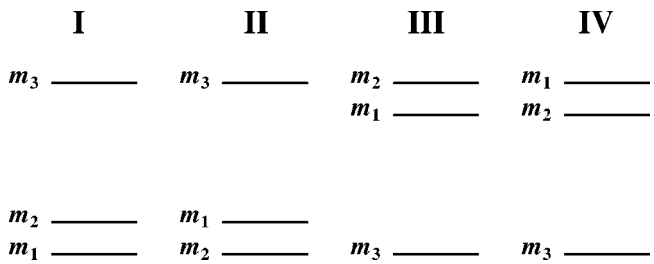

FIG. 1. Schematical view of the four types of neutrino mass hierarchy.

3. Solar-neutrino deficit

Deficit of the solar neutrinos observed at several terrestrial experiments [7,9,10] have been successfully interpreted in terms of the $\nu_e \to \nu_X$ ($\nu_X \neq \nu_e$ or $\overline{\nu_e}$) oscillation

$$P_{\nu_e \to \nu_e} = 1 - \sin^2 2\theta_{\rm SOL} \sin^2\left(\frac{\delta m^2_{\rm SOL}}{4E_\nu} L\right) \tag{2.29}$$

in the following four scenarios [7,9,10].

MSW large-mixing-angle (LMA) solution:

$$0.7 < \sin^2 2\theta_{\rm SOL} < 0.9, \tag{2.30a}$$

$$3\times 10^{-5} < \delta m^2_{\rm SOL}(\text{eV}^2) < 15\times 10^{-5}. \tag{2.30b}$$

MSW small-mixing-angle (SMA) solution:

$$1.2\times 10^{-3} < \sin^2 2\theta_{\rm SOL} < 12\times 10^{-3}, \tag{2.31a}$$

$$0.3\times 10^{-5} < \delta m^2_{\rm SOL}(\text{eV}^2) < 1\times 10^{-5}. \tag{2.31b}$$

MSW low-δm^2 (LOW) solution:

$$0.8 < \sin^2 2\theta_{\rm SOL} \leqslant 1, \tag{2.32a}$$

$$10^{-8} < \delta m^2_{\rm SOL}(\text{eV}^2) < 2.5\times 10^{-7}. \tag{2.32b}$$

Vacuum oscillation (VO) solution:

$$\sin^2 2\theta_{\rm SOL} \sim 0.9, \tag{2.33a}$$

$$\delta m^2_{\rm SOL}(\text{eV}^2) \sim 10^{-9}. \tag{2.33b}$$

The SK Collaboration reported that their data on the energy spectrum and the day-night asymmetry disfavor the SMA solution at 95% C.L. Recently the SNO Collaboration gave us the first direct indication of a non-electron and active flavor component in the solar neutrino flux. Because $\delta m^2_{\rm ATM} \gg \delta m^2_{\rm SOL}$ the ν_e survival probability in the three-neutrino model can be expressed as

$$P_{\nu_e \to \nu_e} = 1 - 2|U_{e3}|^2(1-|U_{e3}|^2) - 4|U_{e1}|^2|U_{e2}|^2 \times \sin^2\left(\frac{\Delta_{12}}{2}\right) + \mathcal{O}\left(\frac{E_\nu}{\delta E_\nu \Delta_{13}}\right), \tag{2.34}$$

where terms of order $[\Delta_{13}(\delta E_\nu/E_\nu)]^{-1}$ in Eq. (2.12) are safely neglected. The energy-independent deficit factor $2|U_{e3}|^2(1-|U_{e3}|^2)$ should be smaller than 5% by the

TABLE I. The four neutrino mass hierarchies and the corresponding sign assignments for δm^2_{12} and δm^2_{13}.

	I	II	III	IV
δm^2_{12}	$+\delta m^2_{\rm SOL}$	$-\delta m^2_{\rm SOL}$	$+\delta m^2_{\rm SOL}$	$-\delta m^2_{\rm SOL}$
δm^2_{13}	$+\delta m^2_{\rm ATM}$	$+\delta m^2_{\rm ATM}$	$-\delta m^2_{\rm ATM}$	$-\delta m^2_{\rm ATM}$

CHOOZ constraint (2.25) if $|\delta m^2_{13}| > 3.5\times 10^{-3}$ eV^2. Because we need only rough estimates of the allowed ranges of the MNS matrix elements,[2] we ignore the small energy-independent deficit factor and interpret the results of the two-flavor analysis Eqs. (2.30a)–(2.33a) by using the identifications

$$4|U_{e1}|^2|U_{e2}|^2 = \sin^2 2\theta_{\rm SOL}, \tag{2.35a}$$

$$|\delta m^2_{12}| = \delta m^2_{\rm SOL}. \tag{2.35b}$$

By using unitary condition, the independent parameter U_{e2} is obtained as

$$U_{e2} = \{[1-|U_{e3}|^2 - \sqrt{(1-|U_{e3}|^2)^2 - \sin^2 2\theta_{\rm SOL}}]/2\}^{1/2}. \tag{2.36}$$

Here we choose $U_{e1} > U_{e2}$ by convention.

C. Neutrino mass hierarchy

All the above constraints on the three-neutrino model parameters are obtained from the survival probabilities which are even functions of δm^2_{ij}. We have made the identification

$$\delta m^2_{\rm SOL} = |\delta m^2_{12}| \ll |\delta m^2_{13}| = \delta m^2_{\rm ATM}, \tag{2.37}$$

which is valid for all the four scenarios of the solar neutrino oscillation.

There are four mass hierarchy cases corresponding to the sign of the δm^2_{ij}, as shown in Fig. 1 and Table I. We name them the neutrino mass hierarchy I, II, III, and IV, respectively.[3]

If the MSW effect is relevant for the solar neutrino oscillation, then the neutrino mass hierarchy cases II and IV are not favored, especially for the LMA and SMA solutions. The hierarchy I may be called ''normal'' and the hierarchy III may be called ''inverted.'' Within the three-neutrino model, there is a study [33] which claims that the normal hierarchy I is favored against the inverted one III from the SN1987A observation, but it is controversial [34]. Terrestrial experiments are needed to determine the neutrino mass hierarchy with confidence.

We notice here that there are two types of mass eigenstate for the neutrinos. The states ν_i with the mass $m_i (i=1,2,3)$ appear in the definition [Eq. (2.2)] of the MNS matrix, whose elements are constrained by the existing experiments that measure essentially the neutrino-flavor survival probabilities. Since the survival probabilities (2.9) do not depend on the sign of the mass-squared differences, these constraints do not depend on the neutrino mass hierarchy. Because the MNS matrix elements are constrained uniquely by the neutrino-flavor survival probabilities, we may call these states ''current-based'' mass eigenstates. We find this basis most convenient for our study in this paper. On the other hand, the ''mass-ordered'' mass eigenstates ν'_i, whose masses satisfy

$$m'_1 < m'_2 < m'_3, \tag{2.38}$$

are useful when studying the high-energy behavior of the neutrino mass matrix [35], the matter effects on the neutrino-flavor oscillation [12,13], and when studying the lepton-number violation effects which are proportional to the magnitudes of the Majorana masses. The relation between the current eigenstates and the two mass eigenstates is

$$\begin{pmatrix} \nu_e \\ \nu_\mu \\ \nu_\tau \end{pmatrix} = V_{\rm MNS} \begin{pmatrix} \nu_1 \\ \nu_2 \\ \nu_3 \end{pmatrix} = V'_{\rm MNS} \begin{pmatrix} \nu'_1 \\ \nu'_2 \\ \nu'_3 \end{pmatrix}, \tag{2.39}$$

where $V'_{\rm MNS}$ is the MNS matrix in the mass-ordered mass-eigenstate base. It can be obtained from $V_{\rm MNS}$ by

$$V'_{\rm MNS} = V_{\rm MNS} O^X \quad (X = {\rm I, II, III, IV}), \tag{2.40}$$

where the permutation matrices O^X

$$O^{\rm I} = \begin{pmatrix} 1 & 0 & 0 \\ 0 & 1 & 0 \\ 0 & 0 & 1 \end{pmatrix}, \quad O^{\rm II} = \begin{pmatrix} 0 & 1 & 0 \\ 1 & 0 & 0 \\ 0 & 0 & 1 \end{pmatrix},$$

$$O^{\rm III} = \begin{pmatrix} 0 & 1 & 0 \\ 0 & 0 & 1 \\ 1 & 0 & 0 \end{pmatrix}, \quad O^{\rm IV} = \begin{pmatrix} 0 & 0 & 1 \\ 0 & 1 & 0 \\ 1 & 0 & 0 \end{pmatrix} \tag{2.41}$$

relate the two mass eigenstates

$$\begin{pmatrix} \nu_1 \\ \nu_2 \\ \nu_3 \end{pmatrix} = O^X \begin{pmatrix} \nu'_1 \\ \nu'_2 \\ \nu'_3 \end{pmatrix}, \tag{2.42}$$

for the neutrino mass hierarchy I, II, III, and IV, respectively.

D. Neutrino oscillation in the Earth matter

Neutrino-flavor oscillation inside matter is governed by the Schrödinger equation

[2] See, for example, more detailed discussions in Ref. [32].

[3] The hierarchy cases II and IV appear in our convention of choosing $U_{e1} > U_{e2}$, Eq. (2.36). They are equivalent to the cases when $U_{e1} < U_{e2}$ while keeping the mass-squared ordering $\delta m^2_{12} = m^2_2 - m^2_1 > 0$.

$$i\frac{\partial}{\partial t}\begin{pmatrix}\nu_e\\ \nu_\mu\\ \nu_\tau\end{pmatrix}=\frac{1}{2E_\nu}\left[H_0+\begin{pmatrix}a&0&0\\0&0&0\\0&0&0\end{pmatrix}\right]\begin{pmatrix}\nu_e\\ \nu_\mu\\ \nu_\tau\end{pmatrix}$$
$$=H\begin{pmatrix}\nu_e\\ \nu_\mu\\ \nu_\tau\end{pmatrix}, \tag{2.43}$$

where H_0 is the Hamiltonian in the vacuum

$$H_0=U\begin{pmatrix}0&0&0\\0&\delta m_{21}^2&0\\0&0&\delta m_{31}^2\end{pmatrix}U^\dagger \tag{2.44}$$

and a is the matter effect term [12]

$$a=2\sqrt{2}G_F n_e E_\nu=7.56\times10^{-5}(\mathrm{eV}^2)\left(\frac{\rho}{\mathrm{g/cm}^3}\right)(E_\nu\ \mathrm{GeV}). \tag{2.45}$$

Here n_e is the electron density of the matter, G_F is the Fermi constant, and ρ is the matter density. In our analysis, we assume that the density of the Earth's crust relevant for the VLBL experiments up to about 2000 km is a constant[4] $\rho=3$ with an uncertainty of $\Delta\rho=0.1$:

$$\rho\ (\mathrm{g/cm}^3)=3.0\pm0.1. \tag{2.46}$$

The Hamiltonian in the matter H is diagonalized as

$$H=\frac{1}{2E_\nu}\tilde{U}\begin{pmatrix}\lambda_1&0&0\\0&\lambda_2&0\\0&0&\lambda_3\end{pmatrix}\tilde{U}^\dagger, \tag{2.47}$$

by the MNS matrix in the matter $\tilde{U}$. The neutrino-flavor oscillation probabilities in the matter

$$P_{\nu_\alpha\to\nu_\beta}=|\tilde{U}_{\beta1}\tilde{U}^*_{\alpha1}+\tilde{U}_{\beta2}e^{-i\tilde{\Delta}_{12}}\tilde{U}^*_{\alpha2}+\tilde{U}_{\beta3}e^{-i\tilde{\Delta}_{13}}\tilde{U}^*_{\alpha3}|^2 \tag{2.48}$$

take the same form as those in the vacuum Eq. (2.7), where the elements $U_{\alpha i}$ are replaced by $\tilde{U}_{\alpha i}$ and the terms Δ_{ij} are replaced by

$$\tilde{\Delta}_{ij}=\frac{\lambda_j-\lambda_i}{2E_\nu}L\equiv\frac{\delta\tilde{m}^2_{ij}}{2E_\nu}L. \tag{2.49}$$

Before closing this section, we give a useful relationship between the $\nu_\alpha\to\nu_\beta$ transition and the $\bar{\nu}_\alpha\to\bar{\nu}_\beta$ transition which may be valid in the terrestrial LBL experiments where both the accelerator and the detectors are near the Earth surface. The oscillation of antineutrinos in matter is given by the Schrödinger equation

$$i\frac{\partial}{\partial t}\begin{pmatrix}\bar{\nu}_e\\ \bar{\nu}_\mu\\ \bar{\nu}_\tau\end{pmatrix}=\left[\bar{H}_0+\begin{pmatrix}-a&0&0\\0&0&0\\0&0&0\end{pmatrix}\right]\begin{pmatrix}\bar{\nu}_e\\ \bar{\nu}_\mu\\ \bar{\nu}_\tau\end{pmatrix}$$
$$=\bar{H}\begin{pmatrix}\bar{\nu}_e\\ \bar{\nu}_\mu\\ \bar{\nu}_\tau\end{pmatrix}. \tag{2.50}$$

The Hamiltonian in the vacuum is identical to the one governing the neutrino-flavor oscillation (2.44)

$$\bar{H}_0=\frac{1}{2E}U^\dagger\begin{pmatrix}0&0&0\\0&\delta m_{21}^2&0\\0&0&\delta m_{31}^2\end{pmatrix}U=H_0^\dagger=H_0. \tag{2.51}$$

By comparing the total Hamiltonians H and $\bar{H}$

$$H=\frac{\delta m_{13}^2}{2E}\left[\begin{pmatrix}\frac{2aE}{\delta m_{13}^2}+|U_{e3}|^2&U_{e3}U^*_{\mu3}&U_{e3}U^*_{\tau3}\\U_{\mu3}U^*_{e3}&|U_{\mu3}|^2&U_{\mu3}U^*_{\tau3}\\U_{\tau3}U^*_{e3}&U_{\tau3}U^*_{\mu3}&|U_{\tau3}|^2\end{pmatrix}+\frac{\delta m_{12}^2}{\delta m_{13}^2}\begin{pmatrix}|U_{e2}|^2&U_{e2}U^*_{\mu2}&U_{e2}U^*_{\tau2}\\U_{\mu2}U^*_{e2}&|U_{\mu2}|^2&U_{\mu2}U^*_{\tau2}\\U_{\tau2}U^*_{e2}&U_{\tau2}U^*_{\mu2}&|U_{\tau3}|^2\end{pmatrix}\right], \tag{2.52a}$$

$$\bar{H}=\frac{\delta m_{13}^2}{2E}\left[\begin{pmatrix}-\frac{2aE}{\delta m_{13}^2}+|U_{e3}|^2&U^*_{e3}U_{\mu3}&U^*_{e3}U_{\tau3}\\U^*_{\mu3}U_{e3}&|U_{\mu3}|^2&U^*_{\mu3}U_{\tau3}\\U^*_{\tau3}U_{e3}&U^*_{\tau3}U_{\mu3}&|U_{\tau3}|^2\end{pmatrix}+\frac{\delta m_{12}^2}{\delta m_{13}^2}\begin{pmatrix}|U_{e2}|^2&U^*_{e2}U_{\mu2}&U^*_{e2}U_{\tau2}\\U^*_{\mu2}U_{e2}&|U_{\mu2}|^2&U^*_{\mu2}U_{\tau2}\\U^*_{\tau2}U_{e2}&U^*_{\tau2}U_{\mu2}&|U_{\tau3}|^2\end{pmatrix}\right], \tag{2.52b}$$

we find

$$-\bar{H}^*(\delta m_{12}^2,\delta m_{13}^2)=H(-\delta m_{12}^2,-\delta m_{13}^2). \tag{2.53}$$

[4]A more detailed study should use the "preliminary earth reference model" [36]. We adopt a constant matter density in this report, which may be justified for LBL experiments up to about 2000 km baseline according to the studies in Ref. [37].

TABLE II. Comparison of accelerator parameters used for LBL projects.

	Energy (GeV)	Intensity (10^{12} ppp)	Rep. rate (Hz)	Power (MW)
J-PARC-PS	50	330	0.275	0.75
NuMI	120	40	0.53	0.41
KEK-PS	12	6	0.45	0.0052

Because the Hamiltonian $-\bar{H}^*$ governs the oscillation in the reversed time direction, we find that the following identities hold

$$P^{\mathrm{I}}_{\bar{\nu}_\alpha \to \bar{\nu}_\beta} = P^{\mathrm{IV}}_{\nu_\alpha \to \nu_\beta}, \tag{2.54a}$$

$$P^{\mathrm{II}}_{\bar{\nu}_\alpha \to \bar{\nu}_\beta} = P^{\mathrm{III}}_{\nu_\alpha \to \nu_\beta}, \tag{2.54b}$$

$$P^{\mathrm{III}}_{\bar{\nu}_\alpha \to \bar{\nu}_\beta} = P^{\mathrm{II}}_{\nu_\alpha \to \nu_\beta}, \tag{2.54c}$$

$$P^{\mathrm{IV}}_{\bar{\nu}_\alpha \to \bar{\nu}_\beta} = P^{\mathrm{I}}_{\nu_\alpha \to \nu_\beta}, \tag{2.54d}$$

if the matter density along the baseline is symmetric under the reversal of the beam direction, i.e., under the exchange of the injector and the detector. This condition is met approximately for all terrestrial LBL experiments where both the accelerator and the detector are on or near the Earth's surface.

In the following, we therefore give results for all the four hierarchy patterns but only for the neutrino beam. Oscillation probabilities for antineutrino beams are then obtained according to the rule [Eq. (2.54)], while the CC and neutral-current (NC) event rates are obtained after multiplying the ratio of the anti-neutrino and neutrino cross sections on the target.

III. NARROW-BAND NEUTRINO BEAMS WITH J-PARC PS

A. The KEK-JAERI joint project

The KEK-JAERI joint project J-PARC is a proton accelerator complex and associated experimental facilities which are being constructed in the site of JAERI, Tokai-village, 60 km northeast of KEK. The project consists of 400 MeV Linac, 3 and 50 GeV synchrotrons. The design parameters of 50 GeV proton synchrotron (J-PARC PS) are listed in Table II together with some other proton machines for LBL experiments. The intensity is 3.3×10^{14} protons/pulse (ppp) and the repetition rate is 0.275 Hz. The power reaches 0.75 MW which is 2 orders of magnitudes higher than the KEK 12-GeV PS. The accelerators in the facility will be in the power frontier in the world. The facility was approved by the Japanese government in December, 2000 and the construction will take 6 years from 2001.

In the following discussion, 10^{21} protons on target (POT) is adopted as a typical 1 year operation. This corresponds to about 100 days of operation with the design intensity.

B. Neutrino beams for LBL experiment between J-PARC and SK

As a first stage neutrino experiment at this new facility, long baseline experiment from J-PARC to SK has been planned and discussed seriously by the JHF neutrino working group [19]. Before going into the description of higher energy beam for VLBL experiment, we briefly introduce the beam for the LBL experiment.

Major purposes of the J-PARC-to-SK experiment are (1) precise measurement of oscillation parameters in ν_μ disappearance and (2) to discover ν_e appearance. The principles of the experiment are as follows:

Use of low-energy narrow band beam (NBB) whose peak energy is tuned at the oscillation maximum. Since the distance between J-PARC and SK is 295 km, the peak energy should be around $E_\nu = 0.7$–1.2 GeV for the region of $\delta m^2_{\mathrm{ATM}}$ allowed by the SK observation [6].

Neutrino-energy is kinematically reconstructed event-by-event from the measured lepton momentum by assuming the charged-current quasielastic (CCqe) scattering. Inelastic scattering with invisible secondary hadrons mimic the CCqe interactions and smears the E_ν measurement. Below $E_\nu \sim 1$ GeV, ν_μ interaction is dominated by the CCqe interaction. So the low-energy beam with small high-energy tail is favorable for this method.

Currently, three beam options are being considered, namely, the wide-band beam (WBB), the NBB, and the off-axis beam (OAB).

WBB: Secondary charged pions from production target are focused by two electromagnetic horns [38]. Since the momentum and angular acceptances of the horns are wide, resulting neutrino spectrum are also wide. The advantage of the WBB is the wide sensitivity in δm^2. But backgrounds from inelastic scattering of neutrinos from high-energy neutrinos limit the precision of the oscillation-parameter measurements.

NBB: Two electromagnetic horns have their axis displaced by about $10°$, and an dipole magnet is placed between them to select pion momentum. Resulting spectrum has a sharp peak and much less high energy tail than WBB.

OAB: The arrangement of beam optics is almost the same as WBB, i.e., coaxially aligned two horns. The axis of OAB is intensionally displaced from the SK direction by a few degrees. Pions with various momenta but with a finite angle from the SK direction contribute to a narrow energy region in the ν_μ spectrum [39]. The OAB can produce a factor of 2 or 3 more intense beam than NBB. But unwanted high-energy component is larger than NBB.

The length of the decay pipe is chosen to be relatively short, 80 m for all the configurations. This is because (1) high-energy neutrinos do not improve the measurements, (2) longer pipe costs very much due to the heavy shielding required by the Japanese radiation regulation. In Ref. [19], the WBB is used only in the early stage of the project in order to

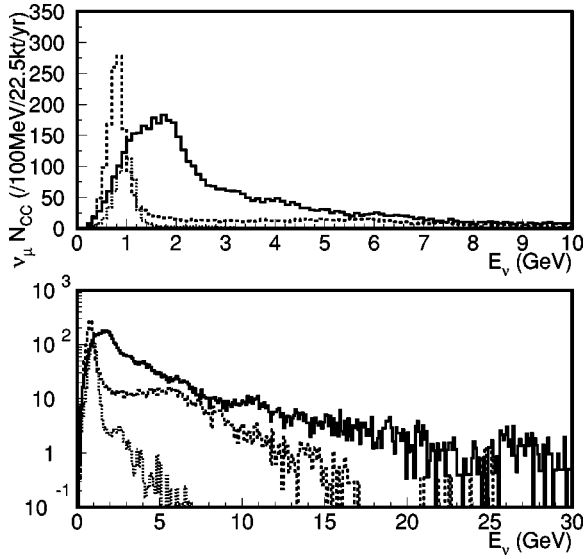

FIG. 2. Typical spectra of the ν_μ CC interactions in the absence of neutrino oscillation in the J-PARC–to–SK LBL experiment. The solid, dashed, and dotted histograms are spectra for WBB, OAB (2 °), and NBB ($\langle p_\pi \rangle = 2$ GeV), respectively.

pin down $\delta m^2_{\rm ATM}$ at about $\sim 10\%$ accuracy.[5] Typical expected spectra of those options are plotted in Fig. 2 and the flux and number of interactions are summarized in Table III.

C. High energy narrow band beam for VLBL experiments

In order to explore the physics potential of the VLBL experiment with J-PARC PS, we need to estimate the neutrino flux whose spectrum has a peak at higher energies. We study the profile of such beams at distances of 1200 km and 2100 km by using Monte Carlo simulation. In this subsection, we describe the beam in detail.

First, we chose the decay pipe length to be 350 m. For the baseline length currently under consideration, 1200 km to Seoul and 2100 km to Beijing, oscillation maximum lies at $E_\nu = 2-4$ GeV and $4-7$ GeV, respectively, for $\delta m^2_{23} = (2-4)\times 10^{-3}$ eV^2. In order to make 5 GeV neutrinos for example, we need pions of momentum about 10 GeV. The 10 GeV pions run about 560 m during their life. Therefore we need a long decay pipe of several 100 m for efficient neutrino production. Considering the site boundary of JAERI and layout of accelerators, maximum decay pipe length is about 350 m.

Secondly, we adopt the NBB configuration. Use of WBB at these high energies has at least two disadvantages.

(i) The reconstruction of neutrino energy is difficult. In the multi-GeV region, ν_μ interactions are dominated by deep-inelastic scattering with multi-pion production. It is difficult for a water Čerenkov detector to make such measurements. It is a nontrivial exercise to construct a 100 kton-level detector of a reasonable cost which has the capability of reconstructing the neutrino energy in the range of several GeV. See, e.g., the proposal in Ref. [27].

(ii) The construction of the beam line costs very much. In the WBB configuration, the proton beam which passes through the production target goes through the decay pipe all the way down. The intensity is still of the order of 10^{14} ppp even beyond the target. In order to shield the extremely high radiation, we need a considerable amount of shielding around the decay pipe. Constructing a decay pipe of several 100 m with heavy shielding is unrealistic.

The OAB also has the second disadvantage. Therefore we choose high energy NBB for the present study, since it does not suffer from the above disadvantages. With an ideal NBB, neutrino energy reconstruction is not necessarily done by the detector. It is possible to design a NBB beam line where the 50 GeV proton beam does not enter the decay pipe. Simulation of high energy WBB is done only for comparison.

For the purpose of focusing secondary pions, we adopt quadrupole (Q) magnets instead of horns. In general, focusing by Q magnets has smaller angular and momentum acceptance than the horn focusing. The reasons why we choose the Q focusing are the following:

(i) Q focusing gives narrower neutrino-energy spectrum.

(ii) High energy pions of ~ 10 GeV are emitted at smaller angles and hence reasonable acceptance for those pions can be obtained by the Q optics.

(iii) The Q-magnet can be operated at low dc current of several kA. Compared with the horn magnets which require pulsed operation with a few 100 kA, much more stable operation can be expected.

We used GEANT [41] for the beam-line simulation to estimate the neutrino flux. A target, Q magnets, a dipole magnet,

TABLE III. Summary of beam simulation of the J-PARC-to-SK LBL experiment. The neutrino flux Φ at SK is in the unit of 10^6/cm^2/yr, and $N_{\rm tot}$ and $N_{\rm CC}$ are the number of total and CC interactions, respectively, in SK's fiducial volume of 22.5 kton for 1 year (10^{21} POT) in the absence of neutrino oscillation.

Beam	$\nu_\mu\Phi$	$\nu_\mu N_{\rm tot}$	$\nu_\mu N_{\rm CC}$	$\nu_e N_{\rm tot}$
NBB ($\langle p_\pi \rangle = 2$ GeV)	7.0	870	620	6.8
OAB(2 °)	19	3100	2200	60
WBB	26	7000	5200	78

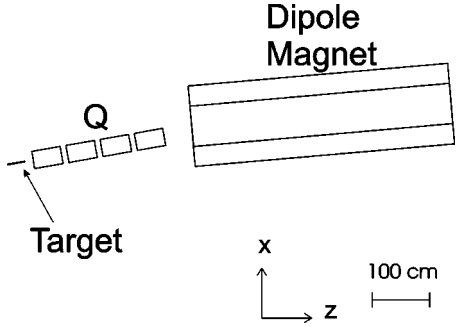

FIG. 3. Beam line optics for high energy narrow band beam.

[5]Very recently the JHF-SK neutrino working group has modified its strategy and the beam configuration. In the most recent plan, the OAB will be adapted for the LBL experiment and the decay pipe length will be 130 m. For more details see Ref. [40].

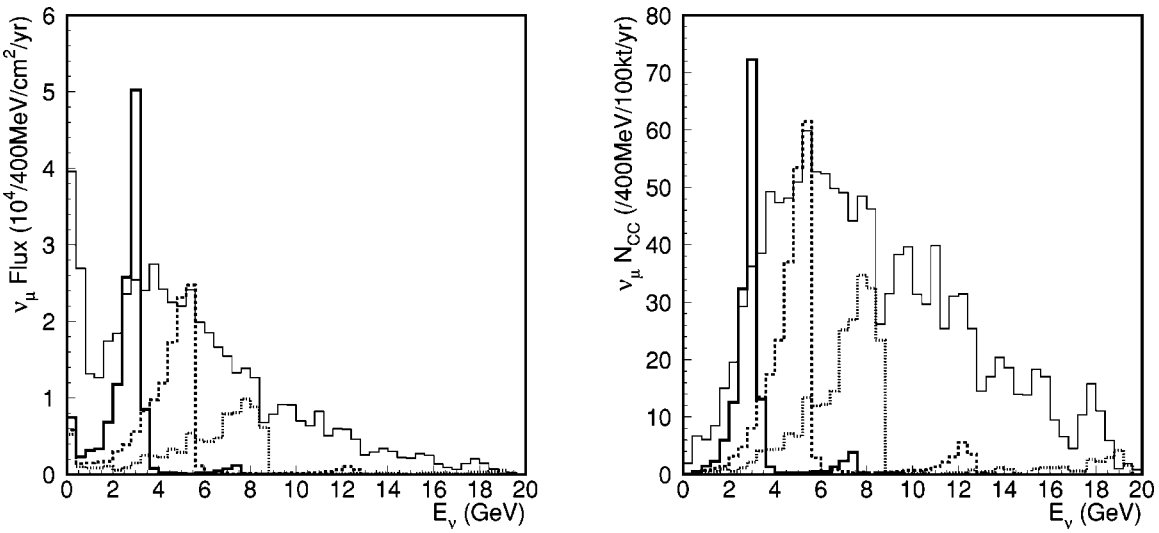

FIG. 4. Typical spectra of narrow band beams. The left figure shows the ν_μ flux and the right one gives the number of ν_μ charged current interactions in the absence of oscillation at $L=2100$ km. The solid, dashed and dotted histograms are 3, 5, and 8 GeV NBB, respectively. The thin solid histograms show the WBB spectra for comparison.

and a decay pipe are put into the geometry. The target is a Cu rod of 1 cm diameter and 30 cm length. The length corresponds to about 2 nuclear interaction lengths. The GCALOR code [42] is used for hadron production in the target. Every secondary particles produced in the target are tracked. The beam line optics assumed for the present study is drawn in Fig. 3. The secondary pions from the target are focused by the following 4 Q magnets and bent by 10° by a dipole magnet. The optics is not fully optimized. Several tens of % increase in flux could be expected by tuning the size or field of the Q and bending magnets, the position of the target, etc.

TABLE IV. Expected number of interactions of ν_μ NBB. Assumed parameters are hierarchy I, $\delta m^2_{\rm ATM}=3.5\times10^{-3}$ eV^2, $\sin^2 2\theta_{\rm ATM}=1.0$, $\delta m^2_{\rm SOL}=10\times10^{-5}$ eV^2, $\sin^2 2\theta_{\rm SOL}=0.8$, $\sin^2 2\theta_{\rm RCT}=0.06$, $\delta_{\rm MNS}=0°$, and $\rho=3$ g/cm^3. First and second lines for each set of baseline length and the peak energy indicate the number of interactions without and with oscillation, respectively.

L	$E_{\rm peak}$	ν_μ CC	$\bar{\nu}_\mu$ CC	ν_e CC	$\bar{\nu}_e$ CC	$N_{\rm NC}$
300 km	3 GeV	7495.0	43.0	55.0	0.90	2540.9
		5903.0	22.0	105.0	1.20	2540.9
	6 GeV	13321.0	44.0	82.0	1.90	4457.4
		12400.0	21.0	110.0	1.70	4457.4
700 km	3 GeV	1376.0	7.9	10.1	0.17	466.7
		382.0	3.8	43.9	0.28	466.7
	6 GeV	2446.0	8.1	15.0	0.35	818.7
		1699.0	3.5	40.6	0.36	818.7
1200 km	3 GeV	468.0	2.7	3.4	0.05	158.8
		85.0	0.8	18.1	0.13	158.8
	6 GeV	833.0	2.7	5.1	0.12	278.6
		297.0	1.1	25.3	0.13	278.6
2100 km	3 GeV	153.0	0.9	1.1	0.02	51.9
		119.0	0.5	2.4	0.05	51.9
	6 GeV	272.0	0.9	1.6	0.04	91.0
		47.0	0.4	13.2	0.06	91.0

In Fig. 4, some typical spectra obtained by the MC simulations are plotted. Spectra with a narrow peak structure are generated. The peak has a sharper edge in the high-energy side than in the low-energy side. The trailing edge in the low-energy side comes from pions with finite angle. We observe a small secondary peak at an energy about twice the primary peak position. The second peak comes from kaon decays. In the left-hand figure, we show the flux of the neutrino at 2100 km away from J-PARC in units of 10^4/400 MeV/cm^2/yr, where 10^{21} POT is assumed for one-year operation. Three types of the NBB where peak energy is at about 3, 5, 8 GeV, and the high-energy WBB spectra are shown. The right-side figures show the expected number of ν_μ CC events per year, in the absence of neutrino oscillation, for a 100 kton detector. The cross section has been obtained by assuming that the target detector is made of water.

Spectra for each neutrino species in the 5 GeV ν_μ and $\bar{\nu}_\mu$ beams are shown in Fig. 5. The flux ratio of ν_e ($\bar{\nu}_e$) to ν_μ ($\bar{\nu}_\mu$) is 0.9% (0.8%) in total, and 0.2% (0.1%) at the peak energy for ν_μ ($\bar{\nu}_\mu$) beam. In the left figure, we show the ν_ν, ν_e, $\bar{\nu}_\mu$, and $\bar{\nu}_e$ spectrum of the NBB ν_μ beam, while in the right figure the corresponding spectrum is shown for the NBB $\bar{\nu}_\mu$ beam. The number of wrong-sign $\bar{\nu}_\mu$ (ν_μ) CC interactions in ν_μ ($\bar{\nu}_\mu$) beam is about 0.4% (4%) of the right-sign interactions. Although the flux of the ν_μ beam and the $\bar{\nu}_\mu$ beam is almost the same, as well as the fraction of contaminated neutrino flux, the $\bar{\nu}_\mu$ beam suffers from 10 times higher wrong-sign events because of a factor of 3 smaller $\bar{\nu}_\mu$ CC interactions than the ν_μ CC interactions off water target at these energies.

The results of the simulations are summarized in Tables IV and V. In Table IV, we show the expected number of CC and NC events for the 3 and 6 GeV ν_μ NBB's for 100 kton yr (10^{21} POT) at four typical distances 300, 700,

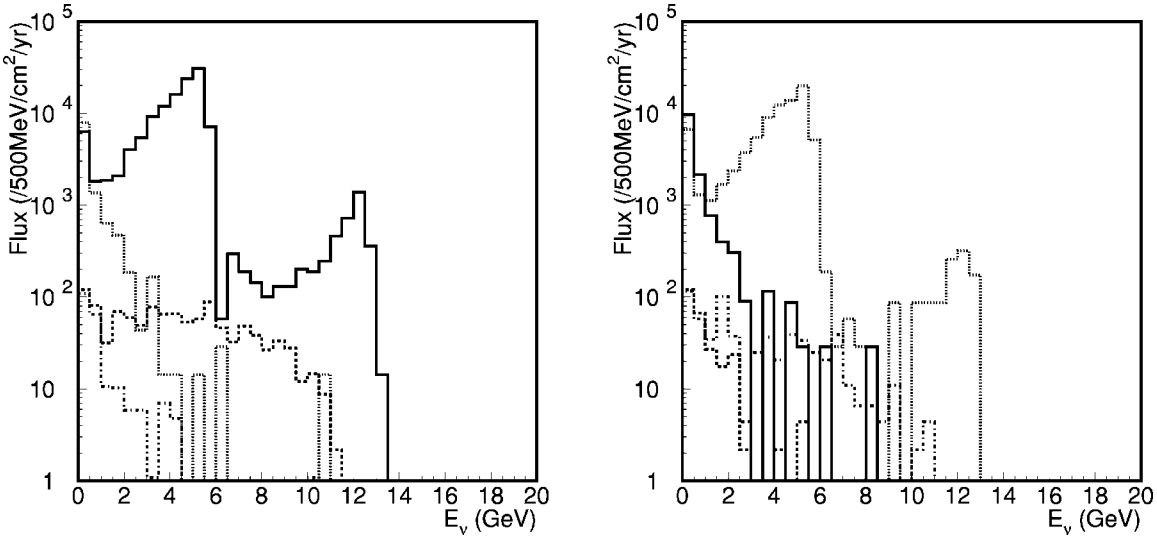

FIG. 5. Composition of neutrino species for a typical NBB. Solid, dashed, dotted, and dot-dashed histograms correspond to ν_μ, ν_e, $\bar{\nu}_\mu$, and $\bar{\nu}_e$, respectively. The left and right figures shows 5 GeV ν_μ and $\bar{\nu}_\mu$ beams, respectively.

1200, and 2100 km from J-PARC. The upper numbers in each row and column show the numbers of events without oscillations, while the lower numbers are calculated by using the three neutrino model for the parameters

$$(\delta m^2_{\rm ATM},\ \delta m^2_{\rm SOL},\ \sin^2 2\theta_{\rm ATM},\ \sin^2 2\theta_{\rm SOL},\ \sin^2 2\theta_{\rm RCT},\ \delta_{\rm MNS}) = (3.5\times 10^{-3},\ 1.0\times 10^{-4},\ 1.0,\ 0.8,\ 0.06,\ 0\,^\circ) \qquad (3.1)$$

with the neutrino mass hierarchy I and for a constant matter density of $\rho=3$ g/cm^3. Because all the three neutrinos have identical NC interactions, the two numbers are identical in $N_{\rm NC}$ column. All the upper numbers simply follow the $1/L^2$ rule of the flux at a distance L.

TABLE V. Expected number of interactions of $\bar{\nu}_\mu$ NBB. Assumed parameters are the same as in Table IV.

L	$E_{\rm peak}$	ν_μ CC	$\bar{\nu}_\mu$ CC	ν_e CC	$\bar{\nu}_e$ CC	$N_{\rm NC}$
300 km	3 GeV	160.0	2871.0	4.0	12.7	1184.7
		66.0	2261.0	4.9	33.6	1184.7
	6 GeV	141.0	4076.0	6.7	13.3	1584.8
		77.0	3793.6	5.4	22.4	1584.8
700 km	3 GeV	29.4	527.0	0.7	2.4	217.6
		13.9	136.0	1.1	16.6	217.6
	6 GeV	25.9	748.6	1.2	2.5	291.1
		11.5	518.5	1.2	10.8	291.1
1200 km	3 GeV	0.0	179.0	0.2	0.8	74.0
		3.5	28.0	0.5	7.0	74.0
	6 GeV	8.8	254.7	0.4	0.8	99.1
		3.4	88.1	0.5	7.5	99.1
2100 km	3 GeV	3.2	58.6	0.1	0.3	24.2
		1.9	47.6	0.2	0.8	24.2
	6 GeV	2.8	83.1	0.1	0.3	32.3
		1.5	12.9	0.2	4.1	32.3

In Table V, we show the corresponding numbers for the $\bar{\nu}_\mu$ NBB's. The number of expected events are about a factor of 3 smaller than the corresponding ones in Table IV because of the smaller CC and NC interactions of $\bar{\nu}_\mu$ off nucleus target. Details of all the NBB's generated for this study are available from Ref. [43].

D. Parametrization of the high-energy NBB

In the numerical studies of the next section, we make the following parametrization of the ν_μ NBB with a single peak at $E_\nu = E_{\rm peak}$:

$$MN_A\Phi(E_\nu)\sigma^{\rm CC}_\mu(E_\nu) = f(E_{\rm peak})\left(\frac{E_\nu}{E_{\rm peak}}\right)^{b(E_{\rm peak})-1}\left(\frac{\sigma^{\rm CC}_\mu(E_\nu)}{\sigma^{\rm CC}_e(E_\nu)}\right), \qquad (3.2)$$

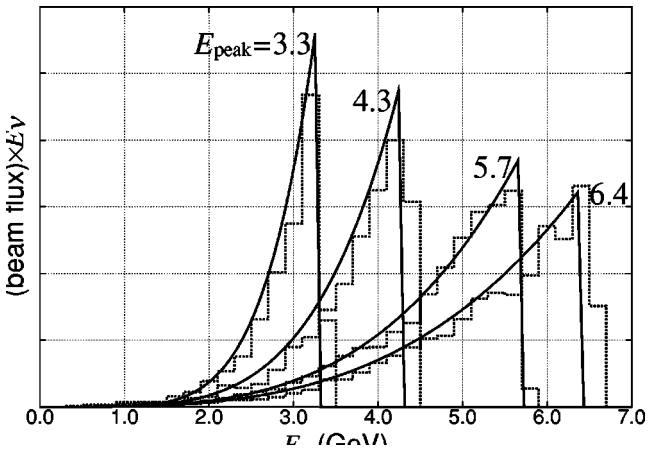

FIG. 6. The NBB's from J-PARC (histograms), and our parametrization (solid lines). The horizontal axis is the neutrino energy (E_ν) and the vertical axis is the beam flux times E_ν.

where $0<E_\nu<E_{\rm peak}$, and $f(E_{\rm peak})$ and $b(E_{\rm peak})$ are parametrized as

$$f(E_{\rm peak})=3.3E_{\rm peak}^2-76.8E_{\rm peak}+520, \tag{3.3a}$$

$$b(E_{\rm peak})=20.3E_{\rm peak}^{-1.4}+2.8. \tag{3.3b}$$

$E_{\rm peak}$ is measured in GeV units, $M=100$ kton stands for the mass of the detector, $N_A=6.017\times10^{23}$ is the Avogadro number, $\Phi(E_\nu)$ is the flux (in units of GeV/cm^2/10^{21} POT) at $L=2100$ km. The $\sigma_\mu^{\rm CC}$ and $\sigma_e^{\rm CC}$ are, respectively, the ν_μ and ν_e CC cross sections per nucleon off water target [44], and their ratio is approximately given by

$$\sigma_\mu^{\rm CC}(E_\nu)/\sigma_e^{\rm CC}(E_\nu) \simeq \begin{cases} 1.0-0.056E_\nu^{-0.48} & (0.7\lesssim E_\nu), \\ 0.83+0.16E_\nu & (0.3\lesssim E_\nu\lesssim 0.7), \\ 0.879(E_\nu-m_\mu)/(0.3-m_\mu) & (m_\mu\lesssim E_\nu\lesssim 0.3), \end{cases} \tag{3.4}$$

where $m_\mu=0.11$ GeV represents the muon mass. This parametrization allows us to study the effects of changing the peak energy of the NBB continuously. We show in Fig. 6 our parametrizations of the NBB neutrino spectra by thick solid curves for several peak energies. For comparison, the corresponding original NBB spectra are shown by histograms. The parametrization reproduces the main part of the ν_μ NBBs well. Because it does not account for the secondary high-energy peak from $K^+\to\mu^+\nu_\mu$ decays (see Fig. 4), we check that our main conclusions are not affected by those details (especially the background from ν_τ CC events).

We have not made parametrizations for the secondary $(\bar{\nu}_\mu,\nu_e,\bar{\nu}_e)$ beams. In the following analysis we use the MC generated secondary beams at discrete energies ($E_{\rm peak}$) [43] and make interpolation for the needed $E_{\rm peak}$ values. Fluxes at different distances and for different species are obtained easily by multiplying the $(2100\ {\rm km}/L)^2$ flux factor and the ratio of the cross section at a given E_ν.

IV. RESULTS

In this section we present results of our numerical studies on physics potential of VLBL experiments by using the NBB's from J-PARC. First, we present our basic strategy of the analysis and explain our simplified treatments of signals and backgrounds, and those of statistical and systematic errors. In the next subsection, we give our reference predictions for the results that may be obtained from the LBL experiment with J-PARC and SK ($L=295$ km). In the latter two subsections, we give results of $L=2100$ km and $L=1200$ km, respectively.

A. Signals, backgrounds, and systematic errors

In order to explore the physics potential of a VLBL experiment with J-PARC at several baseline lengths, we make the following simple treatments in estimating the signals and the backgrounds of a future experiment. For the detector we envisage, a 100 kton-level water-Čerenkov detector which has a capability to distinguish $e^\pm$ CC events from $\mu^\pm$ CC events, but does not distinguish their charges. We do not require capability of the detector to reconstruct the neutrino energy.

Although water-Čerenkov detectors have the capability of measuring the three-momentum of the produced $\mu^\pm$ and $e^\pm$ as well as a part of hadronic activities, we do not make use of the information in our simplified analysis. Instead we use only the total numbers of the produced $\mu^\pm$ and $e^\pm$ events from a NBB with a given peak energy. For each baseline length L, we study the impacts of splitting the assumed total experiment exposure of 1000 kton yr (with 10^{21} POT/yr) into equipartitioned runs of NBB's at several peak energies. We find that the use of two different-energy NBB's improves the physics resolving power of the experiment significantly, but we have not found further improvements by splitting the experiment into more than two NBB's. We therefore choose two appropriate NBB's at each L, whose peak energies are chosen to make physics outputs (such as sensitivity to the neutrino mass hierarchy, $\sin^2 2\theta_{\rm RCT}$ and $\delta_{\rm MNS}$ angles) significant. The optimum choice of NBB's should depend on the model parameters

$$(\delta m^2_{\rm ATM},\delta m^2_{\rm SOL},\sin^2 2\theta_{\rm ATM},\sin^2 2\theta_{\rm SOL},\sin^2 2\theta_{\rm RCT},,\delta_{\rm MNS}), \tag{4.1}$$

especially on $\delta m^2_{\rm ATM}$ and $\sin^2 2\theta_{\rm ATM}$, which will be measured more accurately by K2K [3], MINOS [16], and by J-PARC-to-SK [19] in the future. All our major findings will not be affected by such details as long as appropriate NBB's are chosen according to the data available at the time of the VLBL experiment.

The signals of our analysis are the numbers of ν_μ CC events and those of ν_e CC events from the ν_μ beam. They are calculated as

$$N(\mu,E_{\rm peak},L)=MN_A\int_0^{E_{\rm peak}}dE_\nu\Phi(E_\nu;E_{\rm peak})\sigma_\mu^{\rm CC}P_{\nu_\mu\to\nu_\mu}, \tag{4.2}$$

$$N(e,E_{\rm peak},L)=MN_A\int_0^{E_{\rm peak}}dE_\nu\Phi(E_\nu;E_{\rm peak})\sigma_e^{\rm CC}P_{\nu_\mu\to\nu_e}, \tag{4.3}$$

where the flux at a distance L is calculated from the parametrization at $L=2100$ km [Eq. (3.2)] by multiplying the scale factor $(2100\ {\rm km}/L)^2$. The cross sections are obtained by assuming a pure water target. The probabilities $P_{\nu_\mu\to\nu_\mu}$ and $P_{\nu_\mu\to\nu_e}$ are calculated for the following model parameters:

$$\sin^2 2\theta_{\rm ATM}=1.0,\quad \delta m^2_{\rm ATM}=3.5\times10^{-3}\ {\rm eV}^2, \tag{4.4a}$$

$$\sin^2 2\theta_{\rm SOL}=0.8,\quad \delta m^2_{\rm SOL}=10\times10^{-5}\ {\rm eV}^2, \tag{4.4b}$$

$$\sin^2 2\theta_{\rm RCT}=0.00,0.02,0.04,0.06,0.08,0.10, \tag{4.4c}$$

$$\delta_{\rm MNS}=0^\circ,90^\circ,180^\circ,270^\circ, \tag{4.4d}$$

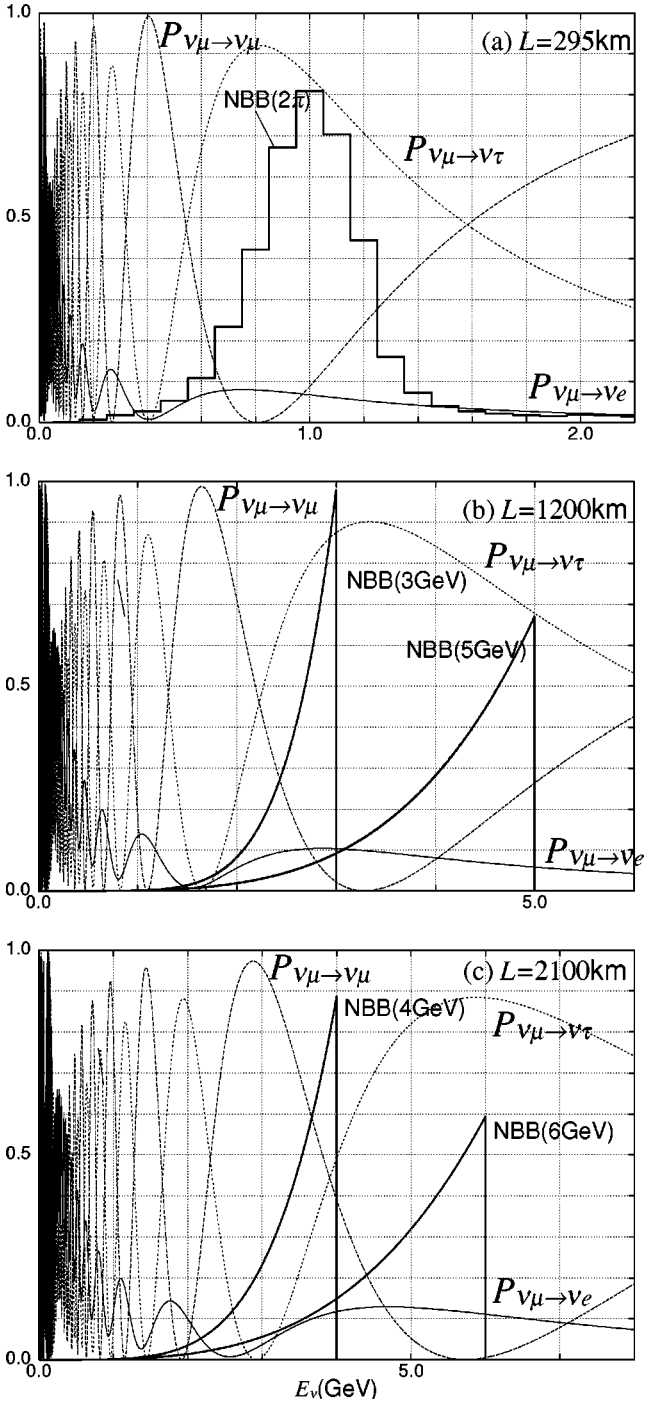

FIG. 7. The neutrino oscillation probabilities at (a) $L=295$ km, (b) $L=1200$ km and (c) $L=2100$ km, calculated for the parameter values $\sin^2 2\theta_{\rm ATM}=1.0$, $\delta m^2_{\rm ATM}=3.5\times10^{-3}$ eV^2, $\sin^2 2\theta_{\rm SOL}=0.8$, $\delta m^2_{\rm SOL}=10\times10^{-5}$ eV^2, $\sin^2 2\theta_{\rm RCT}=0.1$, $\delta_{\rm MNS}=270\,°$, and $\rho=3$ g/cm^3 with the hierarchy I. Overlayed are the NBB's (flux times energy) used in our analysis.

for the neutrino mass hierarchy I

$$\delta m^2_{13}=\delta m^2_{\rm ATM}>0, \quad \delta m^2_{12}=\delta m^2_{\rm SOL}>0 \quad \text{(hierarchy I)}, \tag{4.5}$$

and for a constant matter density

$$\rho=3 \ \ {\rm g/cm}^3. \tag{4.6}$$

We show in Fig. 7 the oscillation probabilities calculated for the above parameters (at $\sin^2 2\theta_{\rm RCT}=0.1$ and $\delta_{\rm MNS}=270\,°$) at three baseline lengths $L=295$ km (SK), $L=1200$ km, and $L=2100$ km. The NBB fluxes ($\times E_\nu$) chosen for our analysis are overlayed in each figure.

The following background contributions to the "μ" and the "e" events are accounted for

$$N(\mu,E_{\rm peak},L)_{\rm BG}=N(\mu;\bar{\nu}_\mu{\rm CC})+N(\mu;\nu_\tau{\rm CC}:\tau\to\mu), \tag{4.7}$$

$$\begin{aligned}N(e,E_{\rm peak},L)_{\rm BG}=&N(e;\nu_e{\rm CC})+N(e;\nu_\tau{\rm CC}:\tau\to e)\\&+N(e;{\rm NC})\\&+N(e;\nu_\tau{\rm CC}:\tau\to \text{ hadrons}).\end{aligned} \tag{4.8}$$

Here $\bar{\nu}_\mu$ CC and ν_e CC contributions are calculated by interpolating the numerical integrations

$$N(l;\overset{(-)}{\nu}_l{\rm CC})=MN_A\int dE_\nu \Phi_{\overset{(-)}{\nu_l}}(E_\nu;E_{\rm peak})\sigma^{\rm CC}_{\overset{(-)}{\nu_l}}P_{\overset{(-)}{\nu_l}\to\overset{(-)}{\nu_l}} \tag{4.9}$$

for the discrete set of the MC simulations [43]. Here $\Phi_{\bar{\nu}_\mu}(E_\nu;E_{\rm peak})$ and $\Phi_{\nu_e}(E_\nu;E_{\rm peak})$ stand for, respectively, the MC generated secondary $\bar{\nu}_\mu$ and ν_e flux of the primarily ν_μ beam. The survival probabilities are calculated for the same set of the model parameters, (4.4). We find that contributions from oscillations from the background beams, such as $\bar{\nu}_e\to\bar{\nu}_\mu$, are negligibly small and hence they are not counted. The contributions from τ-lepton pure-leptonic decays are estimated as

$$\begin{aligned}N(l;\nu_\tau{\rm CC}:\tau\to l)=&MN_A\int dE_\nu\Phi(E_\nu;E_{\rm peak})\\&\times P_{\nu_\mu\to\nu_\tau}\sigma^{\rm CC}_{\nu_\tau}{\rm Br}(\tau\to l\bar{\nu}_l\nu_\tau),\end{aligned} \tag{4.10}$$

where we adopt ${\rm Br}(\tau\to\mu\bar{\nu}_\mu\nu_\tau)=0.1737$ and ${\rm Br}(\tau\to e\bar{\nu}_e\nu_\tau)=0.1783$ [45]. The 10% errors in these branching fractions are accounted for as systematic errors. Because of the τ-lepton threshold, τ backgrounds are significant only at high energies, NBB's with $E_{\rm peak}\gtrsim4$ GeV. Because they receive contribution from the small high-energy secondary peak due to kaon decays, we use the interpolation of the results obtained for the discrete set of MC generated fluxes.

The "e" events receive contributions from the NC events where produced π^0's mimic electron shower in the water-Čerenkov detector. By using the estimations from the SK experiments, we adopt

$$N(e;{\rm NC})=MN_A\int dE_\nu\Phi(E_\nu;E_{\rm peak})\sigma^{\rm NC}_{\nu_\mu}P_{e/{\rm NC}} \tag{4.11}$$

with

$$P_{e/{\rm NC}}=0.0055\pm0.00055. \tag{4.12}$$

TABLE VI. Expected signals and backgrounds for μ-like and e-like events. The results are shown for the parameters of Eq. (4.16) at $\delta_{\rm MNS}=270°$, (a) 500 kton yr at $L=2100$ km, (b) 500 kton yr at $L=1200$ km, (c) 100 kton yr at $L=295$ km.

		$N_{\rm signal}$	$N_{\rm BG}$			$N_{\rm tot}$	$\frac{N_{\rm signal}}{N_{\rm tot}}$
			beams	ν_τ CC	NC		
			(a) $L=2100$ km				
NBB ($E_{\rm peak}=6$ GeV)	$N(\mu)$	202.5	2.2	15.2		219.9	0.92
500 kton yr	$N(e)$	126.5	7.3	15.9	3.3	153.0	.083
NBB ($E_{\rm peak}=4$ GeV)	$N(\mu)$	612.5	2.2	3.5		618.2	0.99
500 kton yr	$N(e)$	66.4	8.5	3.7	2.6	81.2	0.82
			(b) $L=1200$ km				
NBB ($E_{\rm peak}=5$ GeV)	$N(\mu)$	490.1	2.2	8.7		501.0	0.98
500 kton yr	$N(e)$	239.1	10.5	9.0	9.4	268.0	0.89
NBB ($E_{\rm peak}=3$ GeV)	$N(\mu)$	413.8	2.3	0.0		416.1	0.99
500 kton yr	$N(e)$	186.1	4.8	0.0	5.6	196.5	0.95
			(c) $L=295$ km				
NBB ($\langle p_\pi\rangle=2$ GeV)	$N(\mu)$	464.9	7.8	0.0		472.7	0.98
100 kton yr	$N(e)$	161.3	22.0	0.0	7.4	190.7	0.85

The error in the above e/NC misidentification probability is accounted for as a systematic error. The last term in Eq. (4.8) accounts for the probability that the ν_τ CC events with hadronic τ decays are counted as e-like events. In the absence of detailed study of such backgrounds, we use the same misidentification probability for the NC events (4.12) and obtain

$$N(e;\nu_\tau\mathrm{CC}:\tau\to\mathrm{hadrons}) = MN_A\int dE_\nu \Phi(E_\nu;E_{\rm peak}) P_{\nu_\mu\to\nu_\tau}\sigma^{\rm CC}_{\nu_\tau} \times Br(\tau\to\nu_\tau\ \mathrm{hadrons}) P_{e/\rm NC}. \quad (4.13)$$

If the small misidentification probability of Eq. (4.12) holds even for $\tau\to$ hadrons events, their background is only at the 2% level of the $\tau\to e$ background, $N(e;\nu_\tau\mathrm{CC}:\tau\to e)$, and hence can safely be neglected.

In addition, we account for the following two effects as the major part of the systematic uncertainty in the VLBL experiments. One is the uncertainty in the total flux of the neutrino beam, for which we adopt the estimate

$$f_{\rm flux}=1\pm0.03, \quad (4.14)$$

common for all the high-energy NBB's. We allocate an independent flux uncertainty of 3% for the low-energy NBB used for the SK experiment ($L=295$ km) since it uses different optics. Finally, we allocate 3.3% uncertainty in the matter density along the baseline. In our simplified analysis, we use

$$\rho=3.0\pm0.1\ \ \mathrm{g/cm^3} \quad (4.15)$$

as a representative density and the uncertainty.

Typical numbers of expected signals and backgrounds are tabulated in Table VI for the parameter set of Eq. (4.4) at $\sin^2 2\theta_{\rm RCT}=0.1$ and $\delta_{\rm MNS}=270°$. The numerical values are given for the following sets of experimental conditions:

(a) $L=2100$ km, 500 kton yr,

NBB ($E_{\rm peak}=4$ GeV), NBB ($E_{\rm peak}=6$ GeV),

(b) $L=1200$ km, 500 kton yr,

NBB ($E_{\rm peak}=3$ GeV), NBB ($E_{\rm peak}=5$ GeV),

(c) $L=295$ km, 100 kton yr, NBB ($\langle p_\pi\rangle=2$ GeV).

We note here that 100 kton yr at $L=295$ km is what SK can gather in approximately 5 yr with 10^{21} POT per yr. 500 kton yr at longer distances can be accumulated in 5 yr for a 100 kton detector with the same intensity beam.

A few remarks are in order. A 100 kton-level detector at $L=2100$ km or 1200 km can detect comparable numbers of μ-like and e-like events as SK (22.5 kton) at $L=295$ km. The backgrounds due to secondary beams (mostly from the ν_e beam) are significant in all cases for the e-like events. The NC background for the e-like events remains small at high energies if the estimate Eq. (4.12) obtained from the K2K experiment at SK remains valid. We may expect gradual increase in the misidentification probability $P_{e/\rm NC}$ at high energies as the mean multiplicity of π^0 and charged particles grows. Finally the τ-decay background can be significant

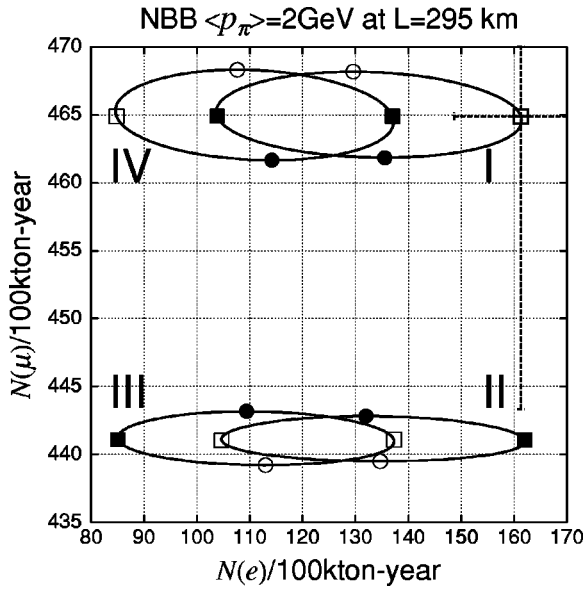

FIG. 8. CP phase dependence of $N(e)$ and $N(\mu)$ at SK ($L=295$ km) for 100 kton yr with the NBB ($\langle p_\pi\rangle=2$ GeV). $\delta_{\rm MNS}=0°$ (solid circle), 90° (solid square), 180° (open circle), and 270° (open square). The results are shown for $\sin^2 2\theta_{\rm ATM}=1.0$, $\delta m^2_{\rm ATM}=3.5\times10^{-3}$ eV^2, $\sin^2 2\theta_{\rm SOL}=0.8$, $\delta m^2_{\rm SOL}=10\times10^{-5}$ eV^2, $\sin^2 2\theta_{\rm RCT}=0.1$, and $\rho=3$ g/cm^3. The predictions for the four types of the neutrino mass hierarchies (Fig. 1) are depicted as I, II, III, and IV.

only for NBB's with $E_{\rm peak}\gtrsim 5$ GeV. If a detector is capable of distinguishing τ events from the ν_e and ν_μ CC events, the overall fit quality improves slightly in the three-neutrino model, because the constraint $P_{\nu_\mu\to\nu_e}+P_{\nu_\mu\to\nu_\mu}+P_{\nu_\mu\to\nu_\tau}=1$ implies that the information obtained from the $P_{\nu_\mu\to\nu_e}$ measurement always diminishes by contaminations from the τ events.

B. Results for $L=295$ km

In Fig. 8 we show the number of ν_μ CC events $N(\mu)$ and that of ν_e CC events $N(e)$ expected at SK ($L=295$ km) for 100 kton yr. The NBB with $\langle p_\pi\rangle=2$ GeV, NBB ($\langle p_\pi\rangle=2$ GeV), with 10^{21} POT/yr has been assumed for simplicity. The three-neutrino model parameters of Eq. (4.4) at $\sin^2 2\theta_{\rm RCT}=0.1$ are assumed, and we take $\rho=3$ g/cm^3, Eq. (4.6). The predictions then depend only on the CP phase parameter $\delta_{\rm MNS}$, and when we vary $\delta_{\rm MNS}$ from 0° to 360°, we have a circle on the plane of $N(\mu)$ vs $N(e)$. The four representative cases $\delta_{\rm MNS}=0°$, 90°, 180°, and 270° are marked by solid circles, solid squares, open circles, and open squares, respectively. The four possible mass hierarchy cases of Fig. 1 are depicted as I, II, III, and IV.

Only the expected event-numbers from the ν_μ beam, Eqs. (4.2) and (4.3), are counted in Fig. 8, so that we can read off the ultimate sensitivity of the experiment from the figure. Statistical errors for such an experiment are shown for the $\delta_{\rm MNS}=270°$ point in the mass hierarchy I circle. We can learn from the figure that if we know all the parameters of the three-neutrino model except for the mass hierarchy and if we know the neutrino-beam flux exactly, then there is a possibility of distinguishing the mass hierarchy I from III. In practice, the LBL experiment between J-PARC and SK can constrain mainly $\delta m^2_{\rm ATM}$ and $\sin^2 2\theta_{\rm ATM}$ from $N(\mu)$, and $\sin^2 2\theta_{\rm RCT}$ from $N(e)$ [19]. Figure 8 shows that those measurements should suffer from uncertainties in the remaining parameters of the three-neutrino model, the neutrino mass hierarchy cases and $\delta_{\rm MNS}$, as are explicitly shown, as well as on the solar-neutrino oscillation parameters $\delta m^2_{\rm SOL}$ and $\sin^2 2\theta_{\rm SOL}$. The next generation of the solar-neutrino observation experiments [46] and KamLAND experiment [47] may further constrain the latter two parameters,[6] but the mass hierarchy (between I and III) and $\delta_{\rm MNS}$ should be determined by the next generation of accelerator-based LBL experiments.

It is hence necessary that all the results from the LBL experiment between J-PARC and SK [19] should be expressed as constraints on the three primary parameters $\delta m^2_{\rm ATM}$, $\sin^2 2\theta_{\rm ATM}$, and $\sin^2 2\theta_{\rm RCT}$, which depend slightly on the three remaining parameters of the three-neutrino model $\delta m^2_{\rm SOL}$, $\sin^2 2\theta_{\rm SOL}$, and $\delta_{\rm MNS}$, as well as on the mass-hierarchy cases. In the following subsections, we show that the data obtained from the LBL experiment between J-PARC and SK ($L=295$ km) are useful in determining the neutrino mass hierarchy, and in some cases even $\delta_{\rm MNS}$, when they are combined with the data from a VLBL experiments ($L=2100$ km or 1200 km) with higher-energy neutrino beams from J-PARC.

Before moving on to studying physics potential of VLBL experiments, it is worth noting that the predictions for the mass hierarchy IV in Fig. 8 represent the prediction for the $\bar{\nu}_\mu\to\bar{\nu}_\mu,\bar{\nu}_e$ oscillation probabilities in the hierarchy I, according to the theorem Eq. (2.54), once the scales are corrected by the factor $\sigma(\bar{\nu}_l N)/\sigma(\nu_l N)$. By comparing the $\delta_{\rm MNS}$ dependences of the circle I and circle IV, we can clearly see that $P_{\nu_\mu\to\nu_e}$ and $P_{\bar{\nu}_\mu\to\bar{\nu}_e}$ interchange approximately by exchanging $\delta_{\rm MNS}=90°$ and 270°. The comparison of ν_μ and $\bar{\nu}_\mu$ oscillation experiments at around $L=295$ km hence has a potential of discovering CP violation in the lepton sector. However, determination of the $\delta_{\rm MNS}$ angle by using the $\bar{\nu}_\mu$ beam from J-PARC needs a much bigger detector than SK [19,49].

C. Results for $L=2100$ km

Figure 9 shows the numbers of ν_μ CC events and that of ν_e CC events expected at the baseline length of $L=2100$ km from J-PARC with 500 kton yr. The expected signal event numbers are shown for (a) the NBB with $E_{\rm peak}=4$ GeV and for (b) the NBB with $E_{\rm peak}=6$ GeV. The parameters of the three neutrino model and the matter density are taken exactly the same as in Fig. 8 :

$$\sin^2 2\theta_{\rm ATM}=1.0,\quad \delta m^2_{\rm ATM}=3.5\times10^{-3}\ {\rm eV}^2, \qquad (4.16a)$$

[6]Inpacts of KamLAND measurements for determining the neutrino model parameters have been studied in Ref. [48].

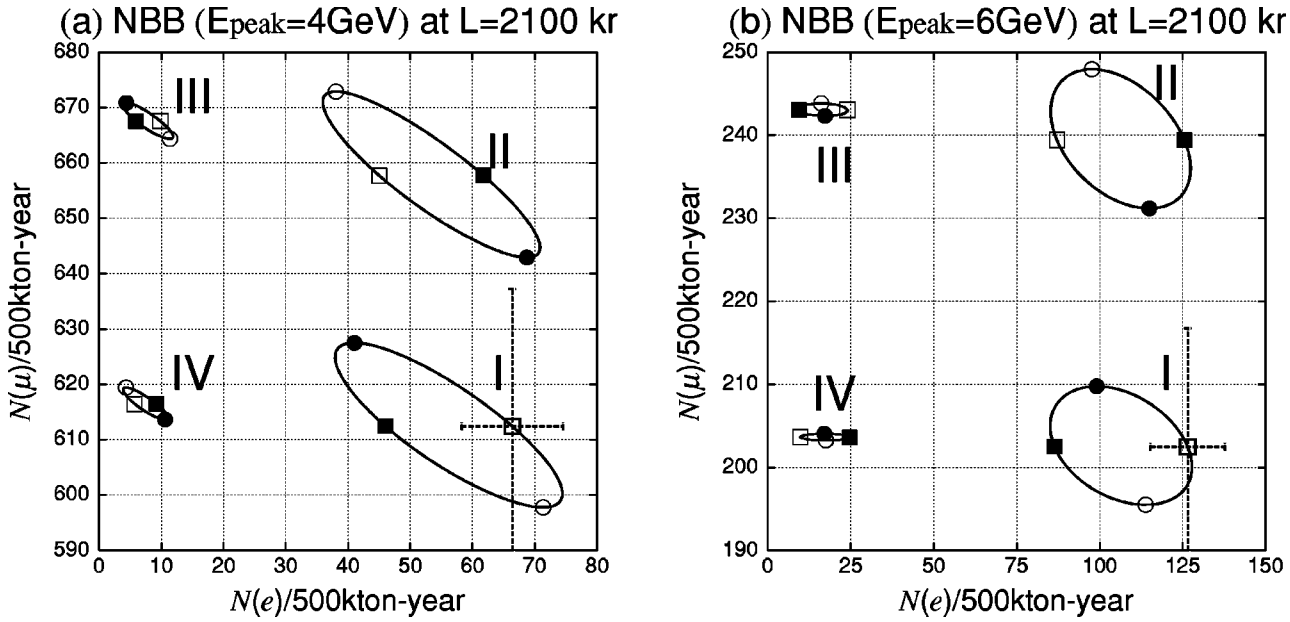

FIG. 9. CP phase dependence of $N(e)$ and $N(\mu)$ at $L=2100$ km for 500 kton yr with (a) NBB ($E_{\rm peak}=4$ GeV) and (b) NBB ($E_{\rm peak}=6$ GeV). $\delta_{\rm MNS}=0\,^\circ$ (solid circle), $90\,^\circ$ (solid square), $180\,^\circ$ (open circle), and $270\,^\circ$ (open square). The results are shown for $\delta m^2_{\rm ATM}=3.5\times10^{-3}$ eV^2, $\sin^2 2\theta_{\rm ATM}=1.0$, $\delta m^2_{\rm SOL}=10\times10^{-5}$ eV^2, $\sin^2 2\theta_{\rm SOL}=0.8$, $\sin^2 2\theta_{\rm RCT}=0.1$, and $\rho=3$ g/cm^3. The predictions for the four types of the neutrino mass hierarchies (Fig. 1) are depicted as I, II, III, and IV.

$$\sin^2 2\theta_{\rm SOL}=0.8,\quad \delta m^2_{\rm SOL}=10\times10^{-5}\ \ {\rm eV}^2, \tag{4.16b}$$

$$\sin^2 2\theta_{\rm RCT}=0.1, \tag{4.16c}$$

$$\delta_{\rm MNS}=0\,^\circ-360\,^\circ, \tag{4.16d}$$

$$\rho=3\ \ {\rm g/cm}^3. \tag{4.16e}$$

The predictions for the four neutrino mass hierarchy cases (Fig. 1) are shown by separate circles when the CP-phase angle $\delta_{\rm MNS}$ is allowed to vary freely. The predictions for the four representative phase values are shown by solid circles ($\delta_{\rm MNS}=0\,^\circ$), solid squares ($90\,^\circ$), open circles ($180\,^\circ$), and open squares ($270\,^\circ$).

When comparing with the $L=295$ km case (Fig. 8), it is most striking to find that the predictions for the ν_e CC events $N(e)$ differs by a factor of 5 or even larger in magnitude between the neutrino mass hierarchy I and III. This is because of the enhancement of the matter effect at high energies. This striking sensitivity of the probability $P_{\nu_\mu\to\nu_e}$ on the mass hierarchy cases is the basis of the capability of distinguishing the cases in VLBL experiments by using the J-PARC PS. On the other hand, we will find that the 5% level differences in $N(\mu)$ between the mass hierarchy cases are not useful for this purpose because $P_{\nu_\mu\to\nu_\mu}$ depends strongly on the parameters $\delta m^2_{\rm ATM}$ and $\sin^2 2\theta_{\rm ATM}$, and also because $N(\mu)$ suffers from the neutrino-beam flux uncertainty (4.14).

We have examined NBB's with various peak energies, and find that the NBB with $E_{\rm peak}=6$ GeV (see Fig. 7) makes $N(e)$ largest while keeping $N(\mu)$ small for the atmospheric-neutrino oscillation parameter of Eq. (4.16a). The ration $N(e)/N(\mu)$ can be as large as 1/2 if $\sin^2 2\theta_{\rm RCT}=0.1$ [Eq. (4.16c)] for the hierarchy case I. The NBB with $E_{\rm peak}=4$ GeV is then chosen because it has the $\delta_{\rm MNS}$ dependence of $N(e)$ which is significantly different from that of the $E_{\rm peak}=6$ GeV case. By comparing the hierarchy I circles of Figs. 9(a) and 9(b), we find that for the NBB with $E_{\rm peak}=4$ GeV, $N(e)$ is largest at around $\delta_{\rm MNS}=180\,^\circ$ (open circles) and smallest at around $\delta_{\rm MNS}=0\,^\circ$ (solid circles), whereas for the NBB with $E_{\rm peak}=6$ GeV, $N(e)$ is largest at around $\delta_{\rm MNS}=270\,^\circ$ (open squares) and smallest at around $\delta_{\rm MNS}=90\,^\circ$ (solid squares).

In Fig. 9, we show the statistical errors of the $N(\mu)$ and $N(e)$ measurements at 500 kton yr on the $\delta_{\rm MNS}=270\,^\circ$ point for the hierarchy case I. The size of the error bars suggest that a 100 kton-level detector is needed to explore the model parameters in VLBL experiments at $L\simeq2100$ km. It also tells us that such detector has the potential of discriminating the neutrino mass hierarchies and constraining the $\delta_{\rm MNS}$ angle in a certain region of the three-neutrino model parameter space. A more careful error analysis that accounts for backgrounds and systematic errors is given in the next subsection.

We are now ready to study the physics capability of such VLBL experiments in some detail. In Fig. 10, we show the expected numbers of signal events $N(\mu)$ and $N(e)$ for the same NBB's and for the same volume of 500 kton yr as in Fig. 9. The circles of Fig. 9 are now made of $36\delta_{\rm MNS}$ points, $\delta_{\rm MNS}=n\times10\,^\circ$ for $n=1$ to 36, for each set of the model parameters. The common parameters for all the points are

$$\sin^2 2\theta_{\rm ATM}=1.0,\quad \delta m^2_{\rm ATM}=3.5\times10^{-3}\ \ {\rm eV}^2, \tag{4.17a}$$

$$\sin^2 2\theta_{\rm RCT}=0.00, 0.02, 0.04, 0.06, 0.08, 0.10, \tag{4.17b}$$

$$\delta_{\rm MNS}=n\times10\,^\circ\ \ (n=1\ \ {\rm to}\ \ 36), \tag{4.17c}$$

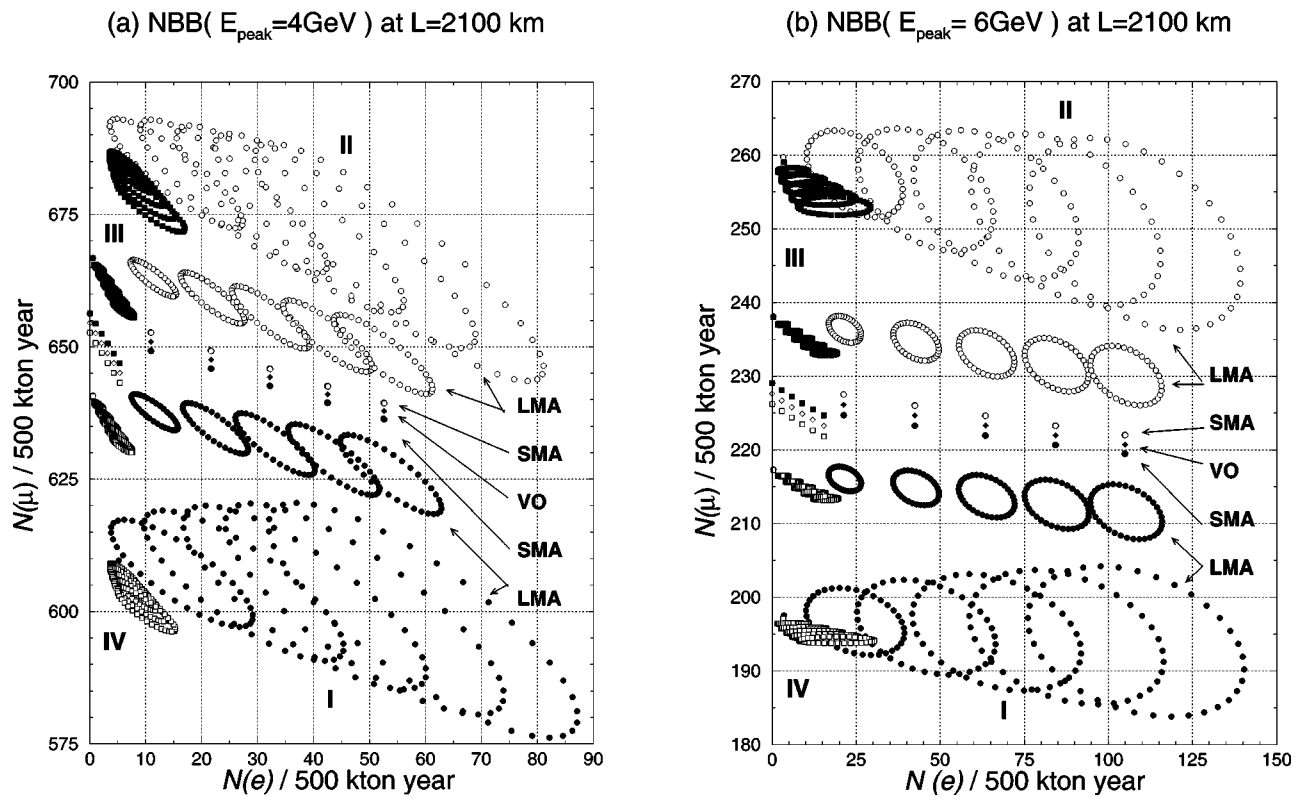

FIG. 10. The neutrino parameter dependences of the expected numbers of ν_e CC and ν_μ CC events $N(e)$ and $N(\mu)$, respectively, for the NBB with $E_{\rm peak}=4$ GeV (a) and 6 GeV (b) with 500 kton yr at $L=2100$ km. The predictions are shown for the LMA, SMA, and VO scenarios of the solar neutrino oscillations and for the four neutrino mass hierarchies I to IV. All the numbers are calculated for $\delta m^2_{\rm ATM}=3.5\times10^{-3}$ eV^2 and $\sin^2 2\theta_{\rm ATM}=1.0$ at $\sin^2 2\theta_{\rm RCT}=0.02\times m(m=0$ to 5) and $\delta_{\rm MNS}=10°\times n(n=1$ to 36). The five larger circles in each hierarchy show the $\delta_{\rm MNS}$ predictions of the LMA with $\delta m^2_{\rm SOL}=15\times10^{-5}$ eV^2 and the five smaller circles are for the LMA with $\delta m^2_{\rm SOL}=5\times10^{-5}$ eV^2, both for $m=1$ to 5. $\delta_{\rm MNS}$ dependence is not recognized for the predictions of SMA and VO, and also at $\sin^2 2\theta_{\rm RCT}=0$ $(m=0)$. The VO predictions are the same for the hierarchy I and II, and III and IV.

$$\rho=3\ \ {\rm g/cm^3}. \tag{4.17d}$$

The predictions for the six $\sin^2 2\theta_{\rm RCT}$ cases (4.17b) can be recognized as five circles and one point with decreasing $N(e)$ values, as $\sin^2 2\theta_{\rm RCT}$ decreases from 0.1 to 0.0. The remaining two parameters are constrained by the solar-neutrino oscillation experiments, and we chose the following representative parameter sets for the three possible solutions to the solar-neutrino deficit anomaly:

$$\text{LMA:}\quad \sin^2 2\theta_{\rm SOL}=0.8,\quad \delta m^2_{\rm SOL}=\begin{cases}15\times10^{-5}\ \ {\rm eV^2},\\ 5\times10^{-5}\ \ {\rm eV^2},\end{cases} \tag{4.18a}$$

$$\text{SMA:}\quad \sin^2 2\theta_{\rm SOL}=7\times10^{-3},\quad \delta m^2_{\rm SOL}=5\times10^{-6}\ \ {\rm eV^2}, \tag{4.18b}$$

$$\text{VO:}\quad \sin^2 2\theta_{\rm SOL}=0.7,\quad \delta m^2_{\rm SOL}=7\times10^{-11}\ \ {\rm eV^2}. \tag{4.18c}$$

The predictions of the four types of the neutrino mass hierarchy I, II, III, IV are indicated explicitly.

The solid-circle points in Fig. 10 show the predictions of all the models with neutrino mass hierarchy I. They reside in the corner at large $N(e)$ and small $N(\mu)$. The five grand circles with smallest $N(\mu)$ give the predictions of the LMA solution for $\delta m^2_{\rm SOL}=15\times10^{-5}$ eV^2, and those with larger $N(\mu)$ are for the LMA with $\delta m^2_{\rm SOL}=5\times10^{-5}$ eV^2. It is clearly seen that the $\delta_{\rm MNS}$ dependence (the size of the grand circles) is larger for larger $\delta m^2_{\rm SOL}$ and for larger $\sin^2 2\theta_{\rm RCT}$ as expected. It is worth pointing out that the LMA scenario with $\delta m^2_{\rm SOL}=15\times10^{-5}$ eV^2 predicts nonzero $N(e),N(e)\simeq5/500$ kton yr even when $\sin^2 2\theta_{\rm RCT}=0$. This is because the ''higher'' oscillation modes of the three-neutrino model grow as $\delta m^2_{\rm SOL}/\delta m^2_{\rm ATM}$ rises. The predictions of the SMA parameters appear just above the upper LMA grand circles, where the $\delta_{\rm MNS}$ dependence (the size of the grand circle) diminishes to zero for each $\sin^2 2\theta_{\rm RCT}$ value. This is expected from the Hamiltonian Eq. (2.52a) that governs the neutrino oscillation in matter, because the $\delta_{\rm MNS}$ dependence of observables diminished whenever the second terms proportional to $\delta m^2_{12}/\delta m^2_{13}$ are much smaller than the first term. The predictions of the VO parameters, which are given by the solid diamonds, are shown just above those of the SMA parameters. Here the $\delta_{\rm MNS}$ dependence vanishes because of the extreme smallness of $\delta m^2_{\rm SOL}/\delta m^2_{\rm ATM}$. By the same token,

we cannot distinguish the VO predictions of the neutrino mass hierarchy I and II. Because the magnitude of $\delta m^2_{\rm SOL}$ is so small, the sign of $\delta m^2_{12} = \pm\,\delta m^2_{\rm SOL}$ does not have observable consequences in terrestrial LBL experiments.

The predictions of the four scenarios of the solar neutrino oscillations [VO, SMA, and two $\delta m^2_{\rm SOL}$ cases of LMA in Eq. (4.18)] with the neutrino mass hierarchy II ($\delta m^2_{12} = -\delta m^2_{\rm SOL}$, $\delta m^2_{13} = \delta m^2_{\rm ATM}$) are shown by open-circle points, which are located in the corner of large $N(e)$ large $N(\mu)$. As explained above, the predictions of the VO scenario do not differ from those for the hierarchy I. The predictions of the SMA scenario appear slightly above those of VO. The two LMA scenario predict larger $N(\mu)$ and give visible $\delta_{\rm MNS}$ dependences, which lead to five grand circles each for the five discrete values of assumed $\sin^2 2\theta_{\rm RCT}$. Again the $\delta_{\rm MNS}$ dependence (the size of the grand circles) is larger for the large $\sin^2 2\theta_{\rm RCT}$ and large $\delta m^2_{\rm SOL}$. Summarizing the predictions of the four scenarios in the neutrino mass hierarchies I and II, both of which have $\delta m^2_{13} = \delta m^2_{\rm ATM} > 0$, $N(e)$ grows linearly with increasing $\sin^2 2\theta_{\rm RCT}$ in all four scenarios and for both hierarchies. The predictions of the hierarchy II differ from those of the hierarchy I only by slightly larger $N(\mu)$ in each scenario. The difference in $N(\mu)$ is largest in the LMA scenarios with $\delta m^2_{\rm SOL} = 15\times 10^{-5}$ eV^2, for which the hierarchy II predicts about 30% (10%) larger $N(\mu)$ than the predictions of the hierarchy I for the NBB with $E_{\rm peak} = 6$ GeV (4 GeV).

All the predictions of the hierarchy cases III and IV have very small $N(e)$. The predictions of the hierarchy III are shown by solid squares and those of the hierarchy IV are shown by open squares. As in the case of hierarchy I vs II, the predictions of the VO scenario do not show visible dependence on the sign of $\delta m^2_{12} = \pm\,\delta m^2_{\rm SOL}$, and its common predictions for the hierarchy III and IV are shown by open-diamonds. Even though compressed to the very small $N(e)$ region, the largest $N(e)$ point is for $\sin^2 2\theta_{\rm RCT} = 0.1$. The predictions of the SMA scenario appear just above (below) the VO points for the hierarchy III (IV). In the LMA scenario, the predictions for $N(\mu)$ increase as $\delta m^2_{\rm SOL}$ grows for the hierarchy III, while $N(\mu)$ decreases with $\delta m^2_{\rm SOL}$ for the hierarchy IV.

By noting that the $\nu_\mu \to \nu_e$ oscillation probability of the hierarchy IV (II) is that of the $\bar{\nu}_\mu \to \bar{\nu}_e$ oscillation probability of the hierarchy I (III), see Eq. (2.54), and by noting that the $\bar{\nu}_e$ CC cross section is a factor of three smaller than the ν_e CC cross section, we can conclude from the figures that the $\bar{\nu}_\mu \to \bar{\nu}_e$ oscillation experiments by using the $\bar{\nu}_\mu$ beam from J-PARC are not effective if the neutrino mass hierarchy is indeed type I. On the other hand, if the inverted hierarchy III is chosen by the nature, experiments with the $\bar{\nu}_\mu$ beam should play a major role.

D. A case study of semiquantitative analysis

Now that the intrinsic sensitivity of the very simple observables $N(\mu, E_{\rm peak})$ and $N(e, E_{\rm peak})$ on the three-neutrino model parameters $\sin^2 2\theta_{\rm RCT}$, $\delta_{\rm MNS}$, $\delta m^2_{\rm SOL}$ and the neutrino mass hierarchy cases are shown clearly in Fig. 10, we would like to examine the capability of such VLBL experiments in determining the model parameters. The following three questions are of our concern.

(1) Can we distinguish the neutrino mass hierarchy cases?

(2) Can we measure the two unknown parameters of the model $\sin^2 2\theta_{\rm RCT}$ and $\delta_{\rm MNS}$?

(3) How much can we improve the measurements of $\delta m^2_{\rm ATM}$ and $\sin^2 2\theta_{\rm ATM}$?

In this subsection we examine these questions for a VLBL experiment at $L = 2100$ km in combination with the LBL experiment of $L = 295$ km between J-PARC and SK.

For definiteness, we assume that the VLBL experiment at $L = 2100$ km accumulates 500 kton yr each with the NBB ($E_{\rm peak} = 6$ GeV) and NBB ($E_{\rm peak} = 4$ GeV). As for the LBL experiment at $L = 295$ km, we assume that 100 kton yr data are obtained for the NBB ($\langle p_\pi \rangle = 2$ GeV). Although this latter assumption does not agree with the present plan of the J-PARC–to–SK project [40] where the OAB may be used in the first stage, we find that essentially the same final results follow as long as the total amount of data at $L = 295$ km are of the order of 500 kton yr. The expected numbers of μ-like and e-like events

$$N(\mu) = N(\mu, E_{\rm peak}, L) + N(\mu, E_{\rm peak}, L)_{\rm BG}, \qquad (4.19)$$

$$N(e) = N(e, E_{\rm peak}, L) + N(e, E_{\rm peak}, L)_{\rm BG}, \qquad (4.20)$$

are tabulated in Table VI for the parameters of Eq. (4.16) at $\delta_{\rm MNS} = 0°$. We see from Table VI that roughly the same number of $\nu_\mu \to \nu_e$ signal events is expected for an experiment at $L = 2100$ km with 500 kton yr and for an experiment at $L = 295$ km with 100 kton yr. This agrees with the naive scaling low of $N \sim 1/L$ at same L/E_ν.

Our program proceeds as follows. For a given set of the three-neutrino model parameters, we calculate predictions of $N(\mu)$ and $N(e)$, including both the signal and the background, with a parametrized neutrino-beam flux and a constant matter density of the Earth ($\rho = 3$ g/cm^3). We assume that the detection efficiencies of the μ-like and e-like events are 100% for simplicity. The statistical errors of each prediction are then simply the square roots of the observed numbers of events $N(\mu)$ and $N(e)$. In our analysis, we account for the following systematic errors: overall flux normalization error of 3%, uncertainty in the matter density along the baseline of 3.3%, relative uncertainty in the misidentification probability $P_{e/\rm NC}$ of 10%, and relative uncertainty in the τ backgrounds of 10%. The χ^2 function of the fit to the LBL experiments may then be expressed as the sum

$$\chi^2 = \chi^2(L = 2100\ \text{km}) + \chi^2(L = 295\ \text{km}), \qquad (4.21)$$

where the first term is

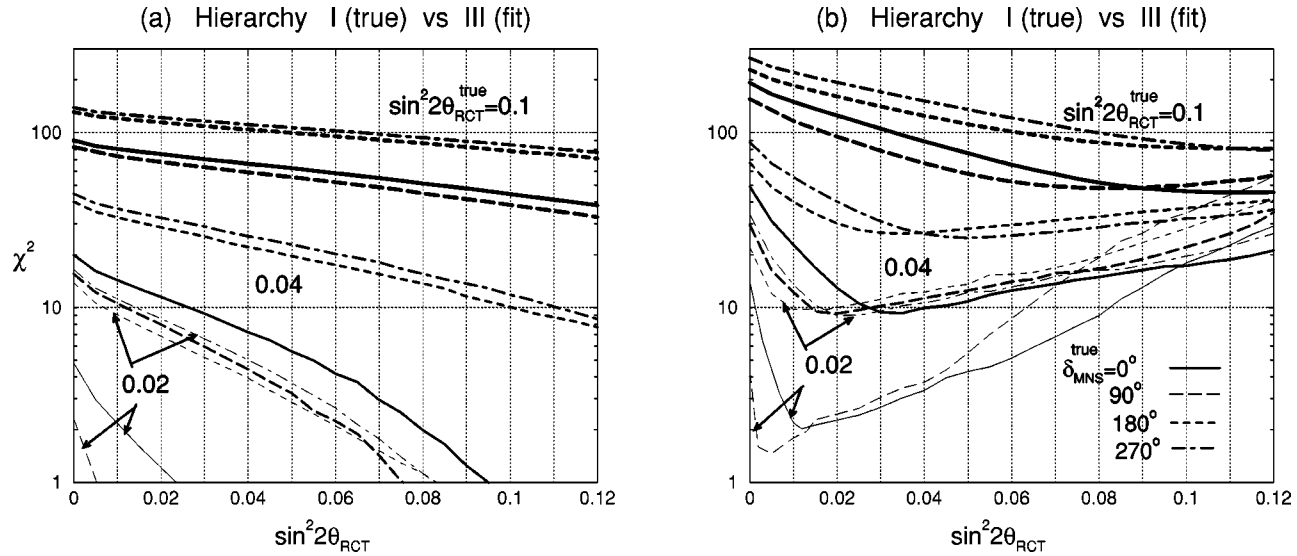

FIG. 11. Minimum χ^2 as functions of the fitting parameter $\sin^2 2\theta_{\rm RCT}$ by assuming the hierarchy III, when the mean values of $N(\mu,E_{\rm peak})$ and $N(e,E_{\rm peak})$ are calculated for the LMA points with hierarchy I [Eq. (4.26)]. In total 12 cases of the input data are labeled by the input ("true") values of $\sin^2 2\theta_{\rm RCT}^{\rm true}=0.02$ (thin lines), 0.04 (medium-thick lines), 0.1 (thick lines), and $\delta_{\rm MNS}^{\rm true}=0°$ (solid lines), 90° (long-dashed lines), 180° (short-dashed lines), 270° (dot-dashed lines). The minimum of the χ^2 function is found by assuming the hierarchy III for a since $\sin^2 2\theta_{\rm RCT}$ value, by varying the parameters $\delta m^2_{\rm SOL}$ and $\sin^2 2\theta_{\rm SOL}$ within the LMA allowed region, and the remaining three parameters $\delta m^2_{\rm ATM}$, $\sin^2 2\theta_{\rm ATM}$, and $\delta_{\rm MNS}$ freely [Eq. (4.27)]. (a) Result with 500 kton yr each for NBB ($E_{\rm peak}=6$ GeV) and NBB ($E_{\rm peak}=4$ GeV) at $L=2100$ km. (b) In addition, 100 kton yr data from NBB ($\langle p_\pi\rangle=2$ GeV) at $L=295$ km are included in the fit.

$$\chi^2(L=2100\ \text{km}) = \sum_{E_{\rm peak},\text{kton yr}} \left\{ \left(\frac{f_{\rm flux}\cdot N^{\rm fit}(\mu)-N^{\rm true}(\mu)}{\sigma(\mu)} \right)^2 + \left(\frac{f_{\rm flux}\cdot N^{\rm fit}(e)-N^{\rm true}(e)}{\sigma(e)} \right)^2 \right\} + \left(\frac{f_{\rm flux}-1}{0.03} \right)^2 + \left(\frac{\rho-3}{0.1} \right)^2, \tag{4.22}$$

$$\sigma(\mu)=\sqrt{N^{\rm true}(\mu)+[0.1N^{\rm true}(\mu;\nu_\tau{\rm CC})]^2}, \tag{4.23}$$

$$\sigma(e) = \sqrt{N^{\rm true}(e)+[0.1N^{\rm true}(e;{\rm NC})]^2+[0.1N^{\rm true}(e;\nu_\tau{\rm CC})]^2}. \tag{4.24}$$

Here the χ^2 is a function of the parameters of the three-neutrino model (the two mass-squared differences, three angles, and one phase), the flux normalization factor $f_{\rm flux}$ and the matter density ρ. We assign the overall flux normalization error of 3% which is common for all high-energy NBB ($E_{\rm peak}$)'s, including the secondary beams. In addition to this common flux normalization error, the individual error of $N(\mu)$ is the sum of the statistical error and the systematic error coming from the uncertainty in the τ background. The error of $N(e)$ is a sum of the statistical error and the systematic errors coming from the uncertainty in the e/NC misidentification probability and the τ background. The χ^2 function for the J-PARC–to–SK experiment is obtained similarly where the 3% flux normalization error and the 3.3% matter density error are assumed to be independent from those for the $L=2100$ km experiment. The function $\chi^2(L=295$ km) is obtained similarly by using the NBB ($\langle p_\pi\rangle=2$ GeV) flux, to which we assign the 3% normalization error.

1. Neutrino mass hierarchy

We show in Fig. 11 the minimum χ^2 as functions of the parameter $\sin^2 2\theta_{\rm RCT}$ by assuming the hierarchy III, when the mean values of $N(\mu,E_{\rm peak})$ and $N(e,E_{\rm peak})$ are calculated for the LMA points with the hierarchy I. The results in Figs. 11(a) and 11(b) are given for the following sets of experimental conditions (A) and (B), respectively.

(A) 500 kton yr each for NBB ($E_{\rm peak}=6$ GeV), and NBB ($E_{\rm peak}=4$ GeV) at $L=2100$ km. (4.25a)

(B) In addition to (A), 100 kton yr data from NBB ($\langle p_\pi\rangle=2$ GeV) at $L=295$ km are included in the fit. (4.25b)

The results are shown for the 12 sets of $N(\mu,E_{\rm peak})$ and $N(e,E_{\rm peak})$, which are generated for the LMA parameters of Eq. (4.4) at $\sin^2 2\theta_{\rm RCT}=0.02,0.04,0.1$, with the matter density $\rho=3$ g/cm^3 by assuming the hierarchy I:

$$\sin^2 2\theta_{\rm ATM}^{\rm true}=1.0, \quad \delta m^{2\,\rm true}_{\rm ATM}=3.5\times10^{-3}\ \text{eV}^2, \tag{4.26a}$$

$$\sin^2 2\theta_{\rm SOL}^{\rm true}=0.8, \quad \delta m^{2\,\rm true}_{\rm SOL}=10\times10^{-5}\ \text{eV}^2, \tag{4.26b}$$

$$\sin^2 2\theta_{\rm RCT}^{\rm true}=0.02,0.04,0.10,$$

$$\delta_{\rm MNS}^{\rm true}=0°,90°,180°,270°, \tag{4.26c}$$

$$\delta m^2_{12}=\delta m^{2\,\rm true}_{\rm SOL}, \quad \delta m^2_{13}=\delta m^{2\,\rm true}_{\rm ATM}\ \text{(hierarchy I)}, \tag{4.26d}$$

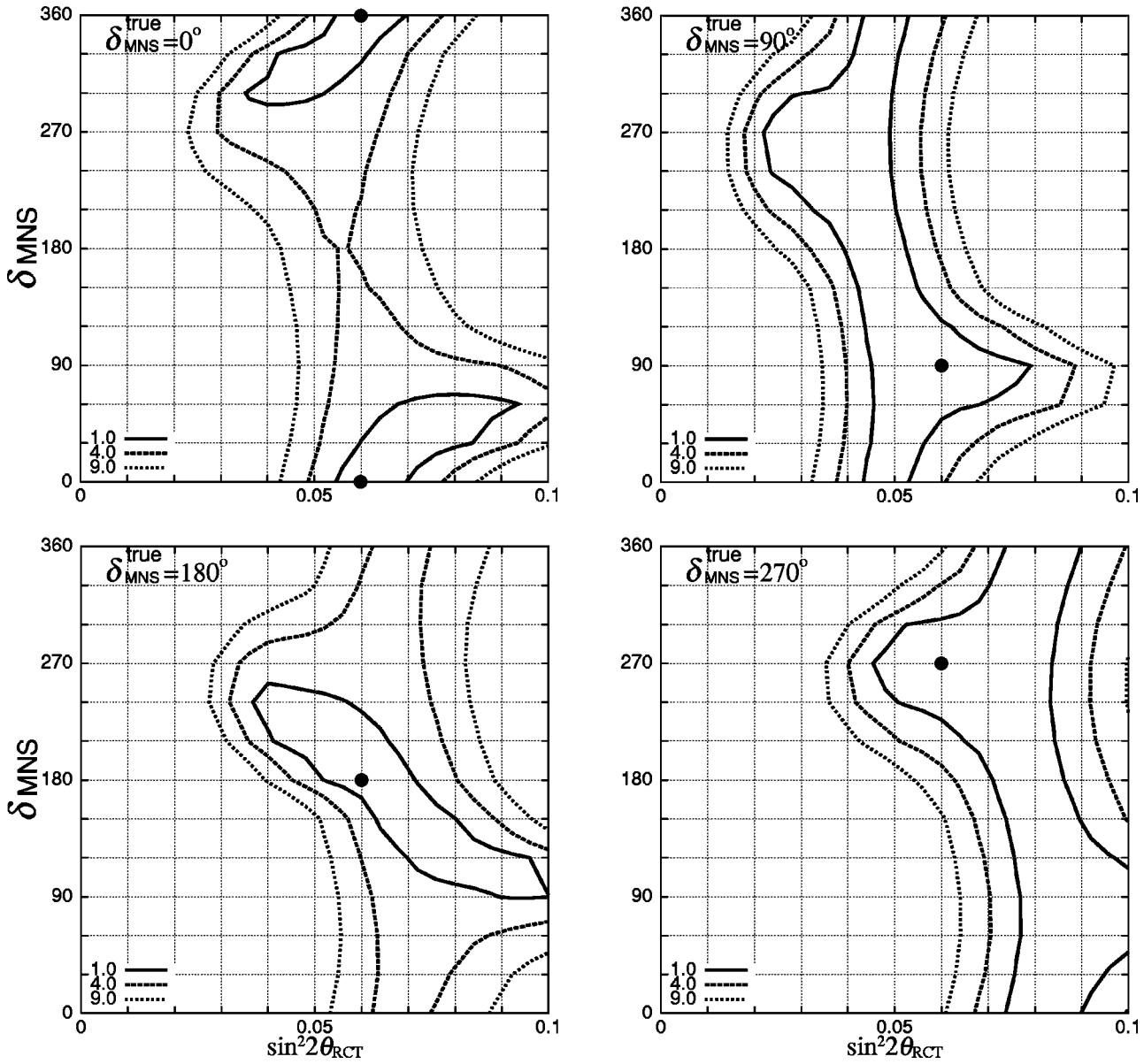

FIG. 12. Regions allowed by the VLBL experiment at $L=2100$ km and the LBL experiment at $L=295$ km, with the experimental condition of Eq. (4.25b). The input data are calculated for the LMA parameters, Eq. (4.26), at $\sin^2 2\theta^{\rm true}_{\rm RCT}=0.06$ and for four values of $\delta^{\rm true}_{\rm MNS}$ 0°, 90°, 180°, and 270°. In each figure, the input parameter point $(\sin^2 2\theta^{\rm true}_{\rm RCT}, \delta^{\rm true}_{\rm MNS})$ is shown by a solid circle, and the regions where $\chi^2_{\rm min}<1$, 4, and 9 are depicted by solid, dashed, and dotted boundaries, respectively.

$$f^{\rm true}_{\rm flux}=1.0, \quad \rho^{\rm true}=3 \ \ {\rm g/cm^3}. \tag{4.26e}$$

The 12 cases of the input data sets are labeled by the input values of $\sin^2 2\theta^{\rm true}_{\rm RCT}=0.02$ (thin lines), 0.04 (medium-thick lines), 0.1 (thick lines), and $\delta^{\rm true}_{\rm MNS}=0°$ (solid lines), 90° (long-dashed lines), 180° (short-dashed lines), 270° (dot-dashed lines).

The χ^2 fit has been performed by assuming the hierarchy III. The minimum of the χ^2 function is found for a $\sin^2 2\theta_{\rm RCT}$ value below 0.12, by varying the parameters $\delta m^2_{\rm SOL}$ and $\sin^2 2\theta_{\rm SOL}$ within the LMA allowed region, Eq. (2.30), and the remaining three parameters $\delta m^2_{\rm ATM}$, $\sin^2 2\theta_{\rm ATM}$, and $\delta_{\rm MNS}$ freely. Summing up, the fitting parameters used to obtain the χ^2 functions of Fig. 11 are

$$\sin^2 2\,\theta_{\rm ATM}: {\rm free}, \quad \delta m^2_{\rm ATM} \ : \ {\rm free}, \tag{4.27a}$$

$$\sin^2 2\,\theta_{\rm SOL}=0.7-0.9,$$

$$\delta m^2_{\rm SOL}=(3-15)\times 10^{-5} \ \ {\rm eV}^2 \ \ ({\rm LMA}), \tag{4.27b}$$

$$\sin^2 2\,\theta_{\rm RCT}: {\rm free}, \quad \delta_{\rm MNS}: {\rm free}, \tag{4.27c}$$

$$\delta m^2_{12}=\delta m^2_{\rm SOL}, \quad \delta m^2_{13}=-\delta m^2_{\rm ATM} \ \ ({\rm hierarchy\ III}), \tag{4.27d}$$

$$f_{\rm flux}: {\rm free}, \quad \rho: {\rm free}. \tag{4.27e}$$

In Fig. 11(a), we show the resulting $\chi^2_{\rm min}$ from the VLBL experiments at $L=2100$ km. The minimum χ^2 for $\sin^2 2\theta^{\rm true}_{\rm RCT}=0.1$ is always larger than 30 for $\sin^2 2\theta_{\rm RCT}<0.12$. We can hence distinguish the neutrino mass hierarchy I from III. At $\sin^2 2\theta^{\rm true}_{\rm RCT}=0.04$, it is possible to make the distinction at more than 3σ level for $\delta^{\rm true}_{\rm MNS}=180°$ and 270°, but not for essentially $\delta^{\rm true}_{\rm MNS}=0°$ and 90°. This is because, the hierarchy I predictions of $N(e)$'s for $\delta^{\rm true}_{\rm MNS}=0°$ and 90° at $\sin^2 2\theta^{\rm true}_{\rm RCT}=0.04$ can be reproduced by the hierarchy-III model if we choose larger $\sin^2 2\theta_{\rm RCT}$ ($\gtrsim 0.08$); see Figs. 9 and 10.

In Fig. 11(b), the minimum χ^2 values are shown when data from J-PARC–to–SK experiment are added. The remarkable difference between Figs. 11(a) and 11(b) is found for the small $\sin^2 2\theta^{\rm true}_{\rm RCT}$ cases when the fitting parameter $\sin^2 2\theta_{\rm RCT}$ is large. This can be explained as follows. In the J-PARC–to–SK LBL experiment, the predicted $N(e,E_{\rm peak})$ of the hierarchy III is not much smaller than that of the hierarchy I (see Fig. 8). In particular, $N(e,E_{\rm peak})$ calculated for the hierarchy I at $\sin^2 2\theta_{\rm RCT}<0.04$ is significantly smaller than that for the hierarchy III at $\sin^2 2\theta_{\rm RCT}>0.1$. This leads to the enhancement of the minimum χ^2 in Fig. 11(b) at large $\sin^2 2\theta_{\rm RCT}$. We find that the data obtained from the J-PARC–to–SK experiments are useful, which allow us to determine the neutrino mass hierarchy (between I and III) for all four values of $\delta^{\rm true}_{\rm MNS}$ at 3σ level when $\sin^2 2\theta^{\rm true}_{\rm RCT}\gtrsim 0.04$, and at one-sigma level when $\sin^2 2\theta^{\rm true}_{\rm RCT}\gtrsim 0.02$.

2. $\sin^2 2\theta_{\rm RCT}$ and $\delta_{\rm MNS}$

Figure 12 shows the regions in the $\sin^2 2\theta_{\rm RCT}$ vs $\delta_{\rm MNS}$ plane which are allowed by the VLBL experiment at $L=2100$ km with 500 kton yr each for NBB ($E_{\rm peak}=6$ GeV) and NBB ($E_{\rm peak}=4$ GeV), together with the 100 kton yr data from the $L=295$ km experiment [Eq. (4.25b)]. The input data are calculated for the LMA parameters [Eq. (4.26)] at $\sin^2 2\theta^{\rm true}_{\rm RCT}=0.1$ and for four values of $\delta^{\rm true}_{\rm MNS}$, 0°, 90°, 180°, and 270°. The χ^2 fit has been performed by assuming that $\delta m^2_{\rm SOL}$ and $\sin^2 2\theta_{\rm SOL}$ are in the LMA region (2.30) while the rest of the parameters are freely varied:

$$\sin^2 2\theta_{\rm ATM}: \quad \text{free}, \quad \delta m^2_{\rm ATM}: \quad \text{free}, \tag{4.28a}$$

$$\sin^2 2\theta_{\rm SOL}=0.7-0.9, \quad \delta m^2_{\rm SOL}=(3-15)\times 10^{-5}\ \text{eV}^2 \quad (\text{LMA}), \tag{4.28b}$$

$$\sin^2 2\theta_{\rm RCT}: \quad \text{free}, \quad \delta_{\rm MNS}: \text{free}, \tag{4.28c}$$

$$\delta m^2_{12}=\delta m^2_{\rm SOL}, \quad \delta m^2_{13}=\delta m^2_{\rm ATM} \ (\text{hierarchy I}), \tag{4.28d}$$

$$f_{\rm flux}: \quad \text{free}, \quad \rho: \quad \text{free}. \tag{4.28e}$$

In each figure, the input parameter point ($\sin^2 2\theta^{\rm true}_{\rm RCT}$, $\delta^{\rm true}_{\rm MNS}$) is shown by a solid circle and the regions where $\chi^2_{\rm min}<1$, 4, and 9 are depicted by solid, dashed, and dotted boundaries, respectively.

A few comments are in order. From the two figures in the right-hand side for $\delta^{\rm true}_{\rm MNS}=90°$ (top) and $\delta^{\rm true}_{\rm MNS}=270°$ (bottom), we learn that $\delta_{\rm MNS}$ cannot be constrained by these experiments. The reason can be qualitatively understood by studying the LMA predictions shown in Figs. 9 and 10. Note, however, that the LMA cases shown in Fig. 10 are for $\delta m^2_{\rm SOL}=5\times 10^{-5}$ and 15×10^{-5} eV^2, while the input data in our example are obtained for $\delta m^2_{\rm SOL}=10\times 10^{-5}$ eV^2. An appropriate interpolation between the two cases is hence needed. From Fig. 9, we find that $\delta_{\rm MNS}=90°$ (solid-square) points for the hierarchy I lie in the lower $N(e)$ corner of the grand circle made of the predictions of all $\delta_{\rm MNS}$. On the other hand, we can tell from Fig. 10 that the same values of low $N(e)$ can be obtained for the other $\delta_{\rm MNS}$ values typically by reducing the $\sin^2 2\theta_{\rm RCT}$ parameter. In case of $\delta^{\rm true}_{\rm MNS}=270°$ (bottom-right), this situation is reversed, and we can expect same $N(e)$ for different $\delta_{\rm MNS}$ by increasing $\sin^2 2\theta_{\rm RCT}$.

The left figures of Fig. 12 show that $\delta_{\rm MNS}$ can be constrained at 1σ level when $\delta^{\rm true}_{\rm MNS}=0°$ (top left) or 180° (bottom left). The reason for this behavior is more subtle. We find that it is essentially the ratio of $N(e,4\ \text{GeV})/N(e,6\ \text{GeV})$ which distinguishes between $\delta_{\rm MNS}=0°$ and 180°. In Fig. 9, we can see that $N(e,4\ \text{GeV})/N(e,6\ \text{GeV})$ is smallest at $\delta_{\rm MNS}=0°$ (solid circles) and it is largest at $\delta_{\rm MNS}=180°$ (open circles), while this ratio is almost the same for $\delta_{\rm MNS}=90°$ (solid squares) and $\delta_{\rm MNS}=270°$ (open squares). Because it is the energy dependence of $N(e)$ that has the discriminating power for $\delta_{\rm MNS}$, detectors with the capability of measuring neutrino energy [27] may have better sensitivity for the $\delta_{\rm MNS}$ angle.

TABLE VII. The mean and the one-sigma errors of $\delta m^2_{\rm ATM}$ and the one-sigma lower bound of $\sin^2\theta^{\rm true}_{\rm ATM}$ when the input data are calculated for the four LMA points [Eq. (4.26) at $\sin^2 2\theta^{\rm true}_{\rm RCT}=0.06$] and the fits are performed by assuming the LMA scenarios. (A) Results with 500 kton yr each for NBB ($E_{\rm peak}=6$ GeV) and NBB ($E_{\rm peak}=4$ GeV) at $L=2100$ km. (B) In addition, 100 kton yr data from NBB ($\langle p_\pi\rangle=2$ GeV) at $L=295$ km are included in the fit.

		$\delta^{\rm true}_{\rm MNS}=0°$	90°	180°	270°
$\delta m^2_{\rm ATM}$	(A)	$3.50^{+0.08}_{-0.10}$	$3.50^{+0.10}_{-0.15}$	$3.50^{+0.11}_{-0.16}$	$3.50^{+0.11}_{-0.15}$
$(\times 10^{-3})(\text{eV}^2)$	(B)	$3.50^{+0.07}_{-0.06}$	$3.50^{+0.09}_{-0.11}$	$3.50^{+0.10}_{-0.10}$	$3.50^{+0.10}_{-0.11}$
$\sin^2\theta_{\rm ATM}$	(A)	0.5 ± 0.077	0.5 ± 0.077	0.5 ± 0.079	0.5 ± 0.077
	(B)	0.5 ± 0.047	0.5 ± 0.047	0.5 ± 0.047	0.5 ± 0.047

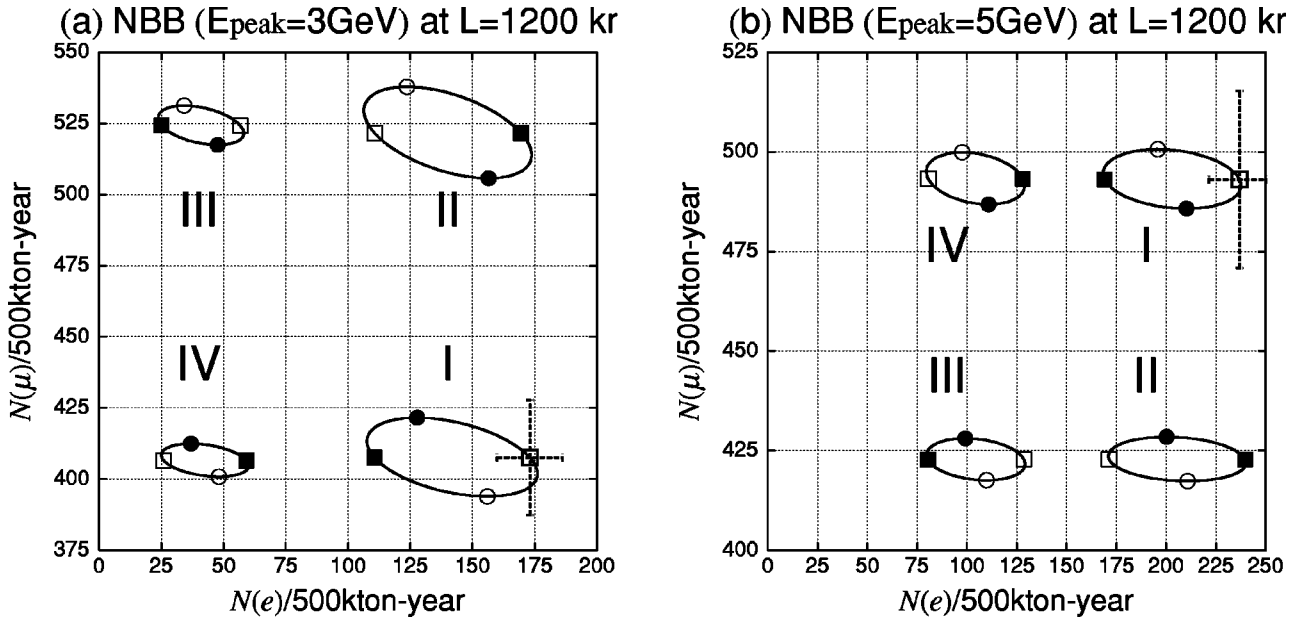

FIG. 13. CP phase dependence of $N(e)$ and $N(\mu)$ at $L=1200$ km for 100 kton yr with (a) NBB ($E_{\rm peak}=3$ GeV) and (b) NBB ($E_{\rm peak}=5$ GeV). $\delta_{\rm MNS}=0\,^\circ$ (solid circle), $90\,^\circ$ (solid square), $180\,^\circ$ (open circle), and $270\,^\circ$ (open square). The input parameters are $\delta m^2_{\rm ATM}=3.5\times10^{-3}$ eV^2, $\sin^2 2\theta_{\rm ATM}=1.0$, $\delta m^2_{\rm SOL}=10\times10^{-5}$ eV^2, $\sin^2 2\theta_{\rm SOL}=0.8$, $\sin^2 2\theta_{\rm RCT}=0.1$, and $\rho=3$ g/cm^3. The predictions for the four types of the neutrino mass hierarchies (Fig. 1) are depicted as I, II, III, and IV.

3. $\delta m^2_{\rm ATM}$ *and* $\sin^2\theta_{\rm ATM}$

Finally, we study the capability of the VLBL experiment in measuring the atmospheric neutrino oscillation parameters $\delta m^2_{\rm ATM}$ and $\sin^2\theta_{\rm ATM}$ accurately. Table VII shows the mean and one-sigma errors of $\delta m^2_{\rm ATM}$ and the one-sigma lower bound on $\sin^2 2\theta^{\rm true}_{\rm ATM}$ when the data are calculated for $\delta m^2_{\rm ATM}=3.5\times10^{-3}$ eV^2 and $\sin^2 2\theta_{\rm ATM}=1.0$ in the LMA scenario with the hierarchy I. The input parameters are chosen for the LMA point of Eq. (4.26), but for $\sin^2 2\theta^{\rm true}_{\rm RCT}=0.06$. The χ^2 fit has been performed by assuming the hierarchy I but allowing all the model parameters to vary freely within the LMA constraint (2.30). The fitting conditions are the same as in Eq. (4.28). The (A) rows gives the results with 500 kton yr each for NBB ($E_{\rm peak}=6$ GeV) and NBB ($E_{\rm peak}=4$ GeV) at $L=2100$ km. The (B) rows gives the results when in addition, 100 kton yr data from NBB ($\langle p_\pi\rangle=2$ GeV) at $L=295$ km are included in the fit. The sensitivities to $\delta m^2_{\rm ATM}$ and $\sin^2 2\theta_{\rm ATM}$ are improved by using the data from the J-PARC–to–SK experiments. The expected sensitivity for $\delta m^2_{\rm ATM}$ is about 3–4.5 % and that for $\sin^2\theta_{\rm ATM}$ is about 15%. After including the J-PARC–to–SK data the sensitivities improve to about 2–3 and 9.4%, respectively.

E. Results for $L=1200$ km

In order to examine the sensitivity of the physics outputs of the VLBL experiments to the baseline length, we repeat the whole analysis for $L=1200$ km, which is approximately the distance between J-PARC and Seoul.

We show in Fig. 13 the expected signal event numbers, $N(e)$ and $N(\mu)$, at the baseline length of $L=1200$ km from J-PARC with 500 kton yr for (a) the NBB with $E_{\rm peak}=3$ GeV and for (b) the NBB with $E_{\rm peak}=5$ GeV. The predictions are calculated for exactly the same three-neutrino model parameters and the matter density as in Figs. 8 and 9, see Eq. (4.16). The predictions for the neutrino mass hierarchy cases I–IV, see Fig. 1 and Table 1, are shown by separate circles when the $\delta_{\rm MNS}$ is allowed to vary freely. The four representative phase values are shown by solid circles ($\delta_{\rm MNS}=0\,^\circ$), solid squares ($90\,^\circ$), open circles ($180\,^\circ$), and open squares ($270\,^\circ$). The statistical errors of the $N(e)$ and $N(\mu)$ measurements at 500 kton yr are shown on the $\delta_{\rm MNS}=270\,^\circ$ point for the hierarchy case I.

Because we have learned from the analysis at $L=2100$ km the number of ν_e CC events $N(e)$ is most sensitive to the neutrino model parameters, we choose the peak energies ($E_{\rm peak}$) of the NBB by requiring large $N(e)$ and suppressed $N(\mu)$. A pair of NBB's is then chosen such that the $\delta_{\rm MNS}$ dependence of the ratio of $N(e)$'s is significant. The chosen peak energies, $E_\nu=3$ and 5 GeV at $L=1200$ km have the same L/E_ν with $E_\nu\simeq5$ and 9 GeV at $L=2100$ km, respectively. In Fig. 13(b) for NBB ($E_{\rm peak}=5$ GeV) at $L=1200$ km, the predicted $N(\mu)$ in the hierarchy I is larger than that in the hierarchy III because the survival probability $P_{\nu_\mu\to\nu_\mu}$ for the mass hierarchy I is smaller than that for the hierarchy III in the interval 3 GeV $\lesssim E_\nu\lesssim6$ GeV. It turns out that this reversing of the ordering of $N(\mu)$ is not very effective in distinguishing the neutrino hierarchy cases because the trend can easily be accounted for by shifting the atmospheric neutrino oscillation parameters $\delta m^2_{\rm ATM}$ and $\sin^2\theta_{\rm ATM}$ slightly.

When we compare Fig. 13 for $L=1200$ km with Fig. 9 for $L=2100$ km, we notice that the reduction of $N(e)$ for the hierarchy III at $L=1200$ km is not as drastic as the reduction at $L=2100$ km, but that the expected statistical errors of the signal are smaller at $L=1200$ km because of a factor of 2

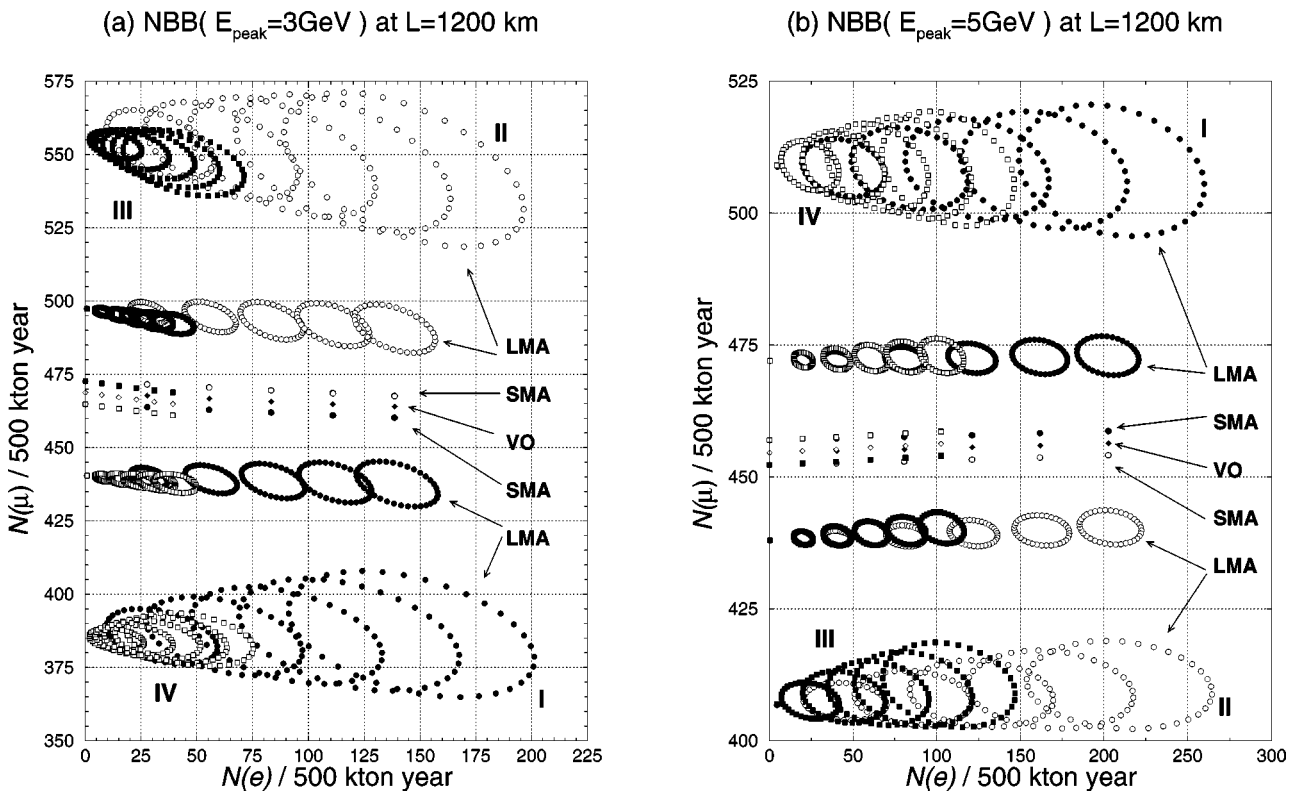

FIG. 14. The neutrino parameter dependences of the expected numbers of ν_e CC events and ν_μ CC events, $N(e)$ and $N(\mu)$, respectively, for the NBB with $E_{\rm peak}=3$ GeV (a) and 5 GeV (b) 500 kton yr at $L=1200$ km. All the symbols are the same as those in Fig. 10.

larger $N(e)$ for the same size of the detector.

In Fig. 14, we show the expected numbers of signal events $N(\mu)$ and $N(e)$ for the same set of NBBs, (a) NBB ($E_{\rm peak}=3$ GeV) and (b) NBB ($E_{\rm peak}=5$ GeV), each with 500 kton yr at $L=1200$ km. The three-neutrino model parameters and the matter density used for calculating those numbers are the same as those used to generate Fig. 10 for $L=2100$ km; see Eqs. (4.17) and (4.18). All the symbols are the same as those adopted in Fig. 10. The dependences of $N(e)$ on the input $\sin^2 2\theta_{\rm RCT}$ are the same as those found in Fig. 10; $N(e)$ decreases as input $\sin^2 2\theta_{\rm RCT}$ is decreased from 0.1 to 0. The solid circles, open circles, solid squares, and open squares show the predictions for the neutrino mass hierarchy I, II, III and IV, respectively. For each hierarchy, the five larger grand circles give the predictions of the LMA scenario with $\delta m^2_{\rm SOL}=15\times10^{-5}$ eV^2, and the smaller circles are for the LMA with $\delta m^2_{\rm SOL}=5\times10^{-5}$ eV^2. The VO predictions of the neutrino mass hierarchies I and II (III

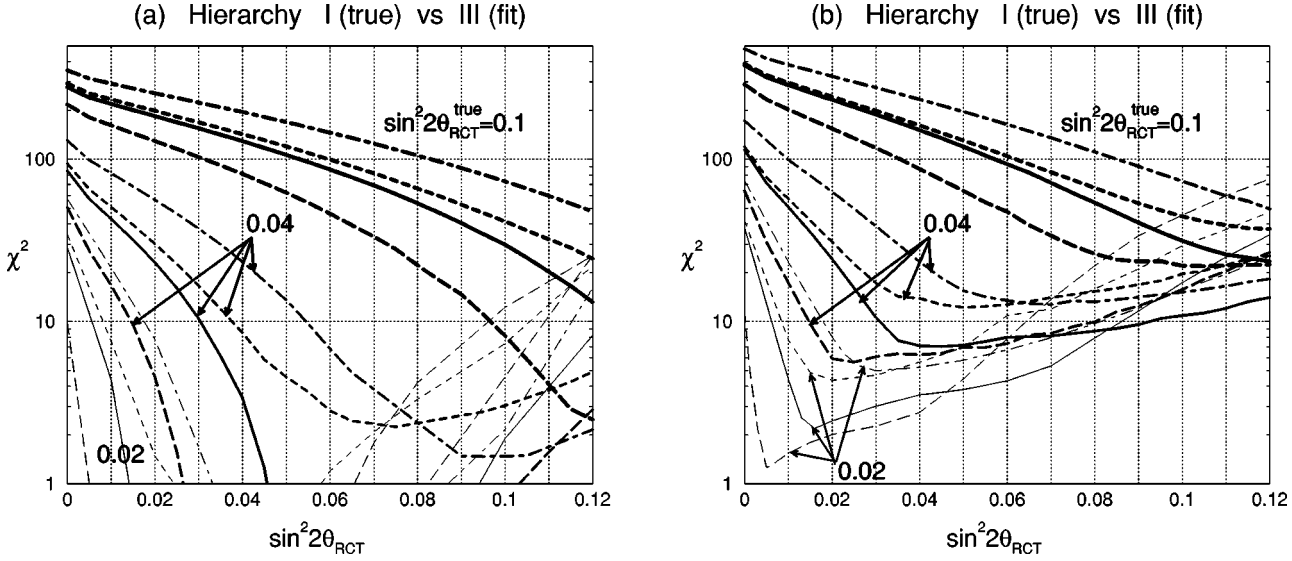

FIG. 15. The same as Figs. 11(a) and 11(b), but for $L=1200$ km.

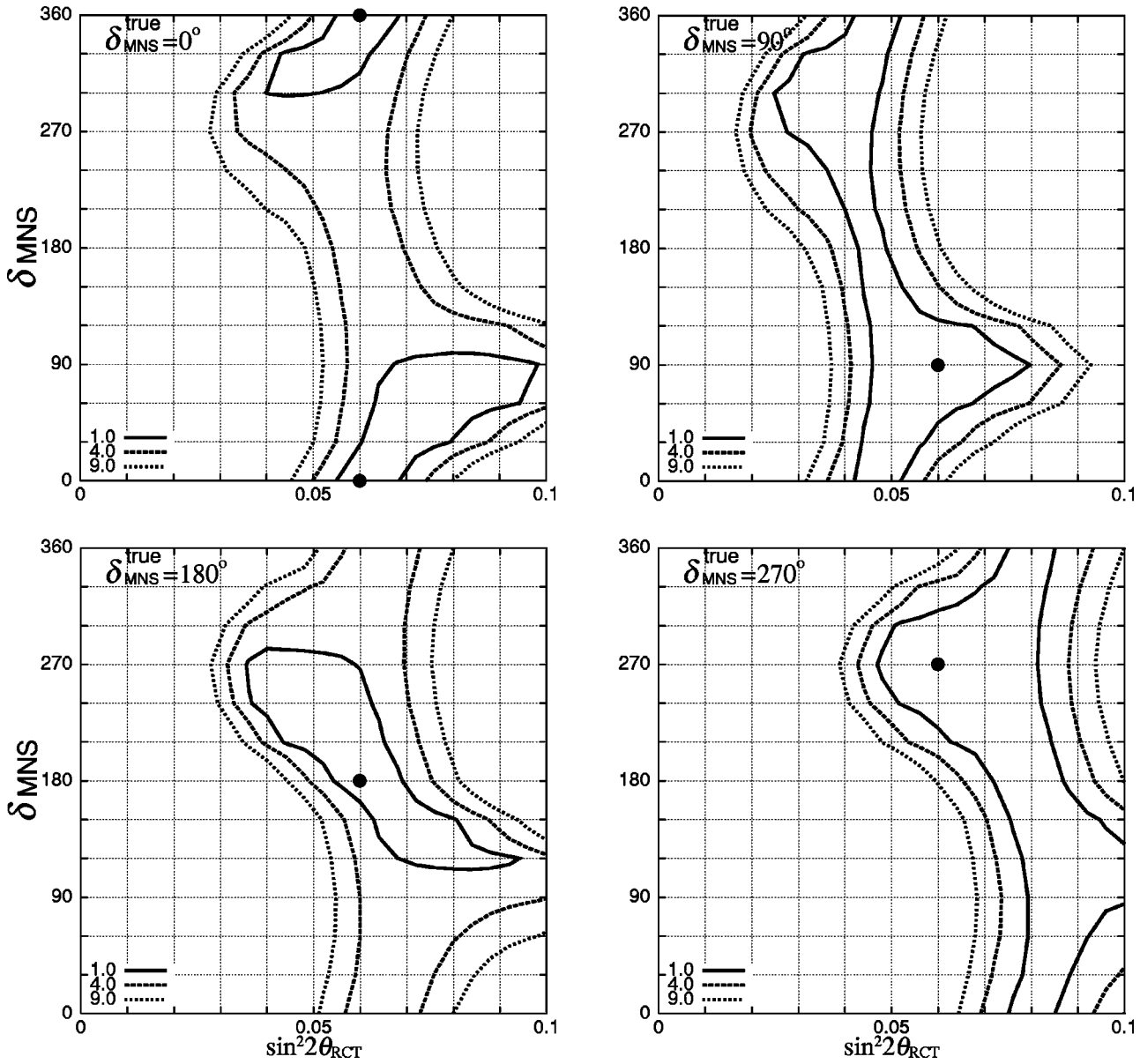

FIG. 16. The same as Fig. 12, but for $L=1200$ km.

and IV) cannot be distinguished, and they are given by the solid (open) diamonds. The difference in $N(\mu)$ is largest in the LMA scenarios with $\delta m^2_{\rm SOL}=15\times10^{-5}$ eV^2, for which the hierarchy III predicts about 40% larger (20% smaller) $N(\mu)$ than the predictions of the hierarchy I for the NBB with $E_{\rm peak}=3$ GeV (5 GeV). When we compare Fig. 14 for $L=1200$ km with the corresponding Fig. 10 for $L=2100$ km, we notice that the prediction for $N(e)$ in the hierarchy III are significantly larger for $L=1200$ km than those for $L=2100$ km. If it were only $N(e)$ in Fig. 14 that effectively discriminates the neutrino mass hierarchy, we should expect significant reduction of the hierarchy discriminating capability of the VLBL experiments at $L=1200$ km.

In order to study these questions quantitatively, we repeat the χ^2 fit for the following sets of experimental conditions:

(A′) 500 kton yr each for NBB ($E_{\rm peak}=5$ GeV) and

NBB ($E_{\rm peak}=3$ GeV) at $L=1200$ km. (4.29a)

(B′) In addition to (A′), 100 kton yr data from

NBB ($\langle p_\pi\rangle=2$ GeV) at $L=295$ km (4.29b)

are included in the fit.

In Figs. 15(a) and 15(b), we show the minimum χ^2 as functions of the fit parameter $\sin^2 2\theta_{\rm RCT}$ for the data sets (A′) and (B′), respectivly. The mean values of $N(\mu,E_{\rm peak})$ and $N(e,E_{\rm peak})$ at $L=1200$ km and those at $L=295$ km are calculated for the experimental conditions of Eq. (4.29) by assuming the LMA scenario and the hierarchy I, and by choosing 12 sets of the model parameters as in Eq. (4.26); $\sin^2 2\theta^{\rm true}_{\rm RCT}=0.02$, 0.04, and 0.10 and $\delta^{\rm true}_{\rm MNS}=0°$, 90°, 180°,

TABLE VIII. The mean and the 1σ errors of $\delta m^2_{\rm ATM}$ and the one-sigma level bound of $\sin^2\theta^{\rm true}_{\rm ATM}$ when the input data are calculated for the four LMA points [Eq. (4.26) at $\sin^2 2\theta^{\rm true}_{\rm RCT}=0.06$] and the fits are performed by assuming the LMA scenarios. (A′) Results with 500 kton yr each for NBB ($E_{\rm peak}=5$ GeV) and NBB ($E_{\rm peak}=3$ GeV) at $L=1200$ km. (B′) In addition, 100 kton yr data from NBB ($\langle p_\pi\rangle=2$ GeV) at $L=295$ km are included in the fit.

		$\delta_{\rm MNS}=0°$	$90°$	$180°$	$270°$
$\delta m^2_{\rm ATM}$	(A′)	$3.50^{+0.065}_{-0.075}$	$3.50^{+0.075}_{-0.08}$	$3.50^{+0.07}_{-0.08}$	$3.50^{+0.085}_{-0.07}$
$(\times 10^{-3})$ (eV^2)	(B′)	$3.50^{+0.065}_{-0.05}$	$3.50^{+0.065}_{-0.075}$	$3.50^{+0.07}_{-0.075}$	$3.50^{+0.07}_{-0.07}$
$\sin^2\theta_{\rm ATM}$	(A′)	0.5 ± 0.039	0.5 ± 0.039	0.5 ± 0.040	0.5 ± 0.040
	(B′)	0.5 ± 0.037	0.5 ± 0.037	0.5 ± 0.037	0.5 ± 0.037

and $270°$. The χ^2 fit has then been performed by assuming the LMA scenario with the hierarchy III; see Eq. (4.27) for details. The 12 lines in Figs. 15(a) and 15(b) correspond to $\sin^2 2\theta^{\rm true}_{\rm RCT}=0.02$ (thin lines), 0.04 (medium-thick lines), 0.1 (thick lines) and $\delta^{\rm true}_{\rm MNS}=0°$ (solid lines), $90°$ (long-dashed lines), $180°$ (short-dashed lines), $270°$ (dot-dashed lines). As in the case of the $L=2100$ km study in Fig. 11, inclusion of the $L=295$ km data improves the sensitivity to the hierarchy cases significantly. After the two experiments are combined, we find that the neutrino mass hierarchy (between I and III) can be distinguished at 3σ level, for all four values of $\delta^{\rm true}_{\rm MNS}$ and when $\sin^2 2\theta_{\rm RCT}=0.1$, and for $\delta^{\rm true}_{\rm MNS}=180°$ and $270°$ when $\sin^2 2\theta^{\rm true}_{\rm RCT}=0.04$. $\chi^2_{\rm min}$ is greater than about 7 for $\delta^{\rm true}_{\rm MNS}=0°$ and $90°$ when $\sin^2 2\theta^{\rm true}_{\rm RCT}=0.04$. Even when $\sin^2 2\theta^{\rm true}_{\rm RCT}=0.02$, $\chi^2_{\rm min}>4$ for $\delta^{\rm true}_{\rm MNS}=180°$ and $270°$. These results at $L=1200$ km are not much worse than the results at $L=2100$ km. We find that this is because the combination of the VLBL experiment and the $L=295$ km LBL experiment is still effective in distinguishing the hierarchy cases, even though the VLBL experiment at $L=1200$ km itself cannot distinguish the hierarchy cases when $\sin^2 2\theta^{\rm true}_{\rm RCT}\lesssim 0.04$.

Figure 16 shows the regions in the $\sin^2 2\theta_{\rm RCT}$ vs $\delta_{\rm MNS}$ plane which are allowed by the VLBL experiments at $L=2100$ km with 500 kton yr each for NBB ($E_{\rm peak}=5$ GeV) and NBB ($E_{\rm peak}=3$ GeV), and the LBL experiment at $L=295$ km with 100 kton yr for NBB ($\langle p_\pi\rangle=2$ GeV) [Eq. (4.29b)]. All the model parameters used to calculate the expected numbers of events and the symbols of the figures are the same as those adopted for Fig. 12. The four input points at $\delta^{\rm true}_{\rm MNS}=0°, 90°, 180°, 270°$ and $\sin^2 2\theta^{\rm true}_{\rm RCT}=0.06$ are shown by the solid circles in each plane, and the region with $\chi^2_{\rm min}<1$, 4, and 9 are shown by the solid, dashed, and dotted boundaries, respectively. The χ^2 fit has been performed by assuming the LMA scenario with the hierarchy I, but otherwise by allowing all the model parameters to vary freely; see Eq. (4.27).

The results shown in Fig. 16 look very similar to those of Fig. 12 for the combination of the VLBL experiment at $L=2100$ km and the LBL experiment at $L=295$ km, Eq. (4.25b). For $\delta^{\rm true}_{\rm MNS}=90°$ and $270°$, we cannot constrain the CP phase at all from these experiments. For $\delta^{\rm true}_{\rm MNS}=0°$ and $180°$, there appear a region of $\chi^2_{\rm min}<1$ where $\delta_{\rm MNS}$ is constrained, but the preferred region covers the whole range at $\chi^2_{\rm min}<4$ level. We find that the area of the $\chi^2_{\rm min}<1$ region is almost the same as that of the $L=2100$ km experiment in Fig. 12 for each $\delta^{\rm true}_{\rm MNS}$ case. We conclude that the capability of measuring $\sin^2 2\theta_{\rm RCT}$ and $\delta_{\rm MNS}$ in the LMA scenario is very similar between the VLBL experiments at $L=2100$ km and those at $L=1200$ km.

Finally, we show in Table VIII the expected accuracy of the measurements of $\delta m^2_{\rm ATM}$ and $\sin^2\theta_{\rm ATM}$. The expected number of events are calculated for $\delta m^{2\,\rm true}_{\rm AMT}=3.5\times10^{-3}$ eV^2 and $\sin^2\theta^{\rm true}_{\rm ATM}=0.5$ in the LMA scenario with the hierarchy I. The 4 LMA input points and the fit parameters are the same as those used for Table VII. The mean and the one-sigma errors for fitted $\delta m^2_{\rm ATM}$ and the one-sigma lower bound for $\sin^2\theta_{\rm ATM}$ are shown in Table VIII. The results of the VLBL experiment only, Eq. (4.29a), are shown in the (A′) row, whereas those obtained by adding the LBL experiment at $L=295$ km, Eq. (4.29b), are shown in the (B′) rows. By comparing the results of Table VII and Table VIII, we find that more precise measurements of $\delta m^2_{\rm ATM}$ and $\sin^2\theta_{\rm ATM}$ can be achieved by the VLBL experiments at $L=1200$ km. This is essentially because the two NBBs that we choose for studying the potential of the $L=1200$ km experiments cover the two sides of the $P_{\nu_\mu\to\nu_\mu}=0$ node, whereas one of the two NBB's chosen for studying the $L=2100$ km case sits on top of the node to minimize $N(\mu)$; see Fig. 7. We find that the accuracy of $\delta m^2_{\rm ATM}$ and $\sin^2\theta_{\rm ATM}$ measurements at the $L=2100$ km experiments can be improved farther, if a NBB with higher peak energy is added. Because higher $E_{\rm peak}$ NBBs give higher τ backgrounds and larger $N(\mu)$, the optimal choice of the beam type and beam energy should be determined according to the prime physics objectives and the details of the proposed detectors.

V. SUMMARY AND DISCUSSIONS

The 50 GeV proton synchrotron at J-PARC (Japan Proton Accelerator Research Complex) [22] will start delivering 10^{21} POT (protons on target) per one operation year by the year 2007. This compares with 3.85×10^{19} POT [50] at 12 GeV which are being provided by the KEK PS for the K2K neutrino oscillation experiment. The J-PARC project thus provides us with an excellent opportunities of extending the K2K experiment, by shooting the neutrino beam from

J-PARC to SK (the Super-Kamiokande) with $L=295$ km [19]. Refinement of the measurements of the atmospheric neutrino oscillation parameters ($\delta m^2_{\rm ATM}$ and $\sin^2\theta_{\rm ATM}$) and the first measurement of the $\nu_\mu \to \nu_e$ oscillation parameter ($\sin^2 2\theta_{\rm RCT}$) by observing the electron appearance are the main targets of the proposed experiment [19].

In this paper, we explored the possibility of extending the LBL experiments to a much longer baseline length ($L>1000$ km) as a second stage of the neutrino oscillation experiments using the J-PARC PS. In particular, we examined in detail the physics potential of VLBL experiments at $L=2100$ km, which is approximately the distance between J-PARC and Beijing, where strong interests in constructing a huge neutrino detector (BAND) have been expressed [27]. We also examined the case at $L=1200$ km carefully in order to study the sensitivity of physics outputs on the baseline lengths of the same order. The distance 1200 km is approximately that between J-PARC and central Korea, where strong interest in LBL neutrino oscillation experiments are expressed.

We studied the physics potential of such VLBL experiments within the three-neutrino model. The three-neutrino model gives a consistent picture of all the neutrino oscillation observations except the LSND experiment, and has six parameters that are observable by neutrino-oscillation phenomena: two mass-squared differences $\delta m^2_{12}=\pm\delta m^2_{\rm SOL}$ and $\delta m^2_{13}=\pm\delta m^2_{\rm ATM}$, three angles $\sin^2 2\theta_{\rm SOL}$, $\sin^2\theta_{\rm ATM}$, and $\sin^2 2\theta_{\rm RCT}$, and one phase $\delta_{\rm MNS}$. The main objectives of such VLBL experiments may be summarized by the following three questions.

(1) Can we distinguish the neutrino mass hierarchy cases?

(2) Can we measure the two unknown parameters of the model $\sin^2 2\theta_{\rm RCT}$ and $\delta_{\rm MNS}$?

(3) How much can we improve the measurements of $\delta m^2_{\rm ATM}$ and $\sin^2 2\theta_{\rm ATM}$?

In order to quantify our answers to the above questions, we make the following simplifications for the neutrino beams and the detector capability.

(i) High-energy NBB's with $E_{\rm peak}=3\sim 6$ GeV for the VLBL experiments.

(ii) Low-energy NBB with $\langle p_\pi\rangle=2$ GeV to represent the LBL experiment to SK.

(iii) 100 kton-level detector which is capable of detecting ν_μ CC and ν_e CC events almost perfectly, but is not necessarily capable of measuring the particle charges and hadron energies.

(iv) Backgrounds from secondary beams and from leptonic τ decays of the ν_τ CC events, as well as those from π^0-e misidentification the neutral current processes are accounted for.

(v) Common flux normalization errors of 3% are assigned for the high-energy NBB's, and an independent 3% error for the low-energy NBB.

(vi) Overall uncertainty in the matter density is assumed to be 3.3% for each experiment.

The detector capabilities of (iii) and (iv) are taken from those of the SK detector which may be common for water-Čerenkov detectors.

We find the following observations. By assuming that the J-PARC–to–SK experiment measures the atmospheric-neutrino oscillation parameters to be centered at $\delta m^2_{\rm ATM}=3.5\times 10^{-3}$ eV^2 and $\sin^2 2\theta_{\rm ATM}=1$, and by assuming that its cumulative effects can be represented by

$$100 \text{ kton yr at } L=295 \text{ km with NBB } (\langle p_\pi\rangle=2 \text{ GeV}), \tag{5.1}$$

we find that VLBL experiments of

$$500 \text{ kton yr at } L=2100 \text{ km with NBB } (E_{\rm peak}=6 \text{ GeV}),$$

$$500 \text{ kton yr at } L=2100 \text{ km with NBB } (E_{\rm peak}=4 \text{ GeV}) \tag{5.2}$$

can give the following answers.

(1) If the neutrino mass hierarchy I is realized in Nature, then the hierarchy III can be rejected at 3σ (1σ) level if $\sin^2 2\theta_{\rm RCT}>0.04$ (0.02), see Fig. 11(b).

(2) If the LMA scenario ($\delta m^2_{\rm SOL}=10\times 10^{-5}$ eV^2, $\sin^2 2\theta_{\rm SOL}=0.8$) is realized in Nature, and if $\sin^2 2\theta_{\rm RCT}=0.06$, then $0.04<\sin^2 2\theta_{\rm RCT}<0.1$ is obtained when $\delta_{\rm MNS}$ is around 0° or 180°, $0.02<\sin^2 2\theta_{\rm RCT}<0.08$ when $\delta_{\rm MNS}$ is around 90°, $0.045<\sin^2 2\theta_{\rm RCT}<0.12$ when $\delta_{\rm MNS}$ is around 270°. $\delta_{\rm MNS}$ can be constrained to local values at one-sigma level when the true $\delta_{\rm MNS}$ is around 0° or 180° but it is unconstrained when it is around 90° or 270°, see Fig. 12.

(3) If the LMA scenario ($\delta m^2_{\rm SOL}=10\times 10^{-4}$ eV^2, $\sin^2 2\theta_{\rm SOL}=0.8$) is realized in Nature, $\delta m^2_{\rm ATM}$ is measured with the 3% accuracy and $\sin^2\theta_{\rm ATM}$ to 9.4% level; see Table VII.

Summing up, a combination of LBL experiments at $L=295$ km and VLBL experiments at $L=2100$ km with the NBBs from J-PARC can determine the neutrino mass hierarchy at the 3σ level if $\sin^2 2\theta_{\rm RCT}>0.04$ can constrain $\sin^2 2\theta_{\rm RCT}$, and it can also constrain $\delta_{\rm MNS}$ at the one-sigma level in some cases. The errors of the atmospheric-neutrino oscillation parameters are reduced to $\delta(\delta m^2_{\rm ATM})=\pm 0.1\times 10^{-3}$ eV^2 and $\sin^2\theta_{\rm ATM}=0.5\pm 0.047$. Very similar results are found for a combination of $L=295$ km and $L=1200$ km experiments; see Figs. 15, 16, and Table VIII.

ACKNOWLEDGMENTS

The authors wish to thank K. Nakamura, J. Sato, Y.F. Wang, K. Whisnant, Z.Z. Xing, C.G. Yang, J.M. Yang, B.L. Young, and X.M. Zhang for stimulating discussions. The works of M.A. and T.K. were supported in part by a Grant-in-Aid for Scientific Research from the Ministry of Education, Culture, Sports, Science and Technology of Japan. K.H. would like to thank the core-university program of JSPS for support. The work of N.O. was supported in part by the U.S. Department of Energy Grant No. DE-FG05-92ER40709.

[1] Kamiokande Collaboration, K. S. Hirata *et al.*, Phys. Lett. B **205**, 416 (1988); **280**, 146 (1992); Y. Fukuda *et al.*, *ibid.* **335**, 237 (1994); IMB Collaboration, D. Casper *et al.*, Phys. Rev. Lett. **66**, 2561 (1991); R. Becker-Szendy *et al.*, Phys. Rev. D **46**, 3720 (1992); SOUDAN2 Collaboration, T. Kafka, Nucl. Phys. B (Proc. Suppl.) **B35**, 427 (1994); M. C. Goodman, *ibid.* **38**, 337 (1995); W. W. M. Allison *et al.*, Phys. Lett. B **391**, 491 (1997); **449**, 137 (1999).

[2] Super-Kamiokande Collaboration, Y. Fukuda *et al.*, Phys. Lett. B **433**, 9 (1998); **436**, 33 (1998); Phys. Rev. Lett. **81**, 1562 (1998).

[3] S. Boyd, Nucl. Phys. B (Proc. Suppl.) **98**, 175 (2001); Y. Oyama, hep-ex/0104014; T. Ishii, hep-ex/0106008; see also the K2K homepage at URL http://neutrino.kek.jp/index.html

[4] CHOOZ Collaboration, M. Apollonio *et al.*, Phys. Lett. B **420**, 397 (1998).

[5] F. Boehm *et al.*, Phys. Rev. Lett. **84**, 3764 (2000); Phys. Rev. D **62**, 072002 (2000); **64**, 112001 (2001).

[6] Super-Kamiokande Collaboration, S. Fukuda *et al.*, Phys. Rev. Lett. **85**, 3999 (2000); hep-ex/0105023; hep-ex/0106025.

[7] Homestake Collaboration, B. T. Cleveland *et al.*, Nucl. Phys. B (Proc. Suppl.) **38**, 47 (1995); Astrophys. J. **496**, 505 (1998); Kamiokande Collaboration, Y. Suzuki, Nucl. Phys. B (Proc. Suppl.) **38**, 54 (1995); Y. Fukuda *et al.*, Phys. Rev. Lett. **77**, 1683 (1996); GALLEX Collaboration, W. Hampel *et al.*, Phys. Lett. B **388**, 384 (1996); SAGE Collaboration, J. N. Abdurashitov *et al.*, Phys. Rev. Lett. **77**, 4708 (1996); Super-Kamiokande Collaboration, Y. Fukuda *et al.*, *ibid.* **81**, 1158 (1998); **82**, 1810 (1999).

[8] J. N. Bahcall, M. H. Pinsonneault, and S. Basu, Astrophys. J. **555**, 990 (2001); see also the homepage of J. N. Bahcall at URL http://www.sns.ias.edu/~jnb/

[9] Super-Kamiokande Collaboration, S. Fukuda *et al.*, Phys. Rev. Lett. **86**, 5656 (2001); **86**, 5651 (2001); hep-ex/0106064.

[10] SNO Collaboration, Q. R. Ahmad *et al.*, Phys. Rev. Lett. **87**, 071301 (2001); **89**, 011301 (2002); **89**, 011302 (2002); see also the SNO Collaboration home page at URL http://www.sno.phy.queensu.ca/

[11] M. Nakagawa, Z. Maki, and S. Sakata, Prog. Theor. Phys. **28**, 870 (1962).

[12] L. Wolfenstein, Phys. Rev. D **17**, 2369 (1978); R. R. Lewis, *ibid.* **21**, 663 (1980); V. Barger, S. Pakvasa, R. J. N. Phillips, and K. Whisnant, *ibid.* **22**, 2718 (1980).

[13] S. P. Mikheyev and A. Yu. Smirnov, Yad. Fiz. **42**, 1441 (1985) [Sov. J. Nucl. Phys. **42**, 913 (1986)]; Nuovo Cimento Soc. Ital. Fis., C **9**, 17 (1986).

[14] B. Pontecorvo, Zh. Eksp. Teor. Fiz. **53**, 1717 (1967); S. M. Bilenky and B. Pontecorvo, Phys. Rep. **41**, 225 (1978); V. Barger, R. J. N. Phillips, and K. Whisnant, Phys. Rev. D **24**, 538 (1981); S. L. Glashow and L. M. Krauss, Phys. Lett. B **190**, 199 (1987).

[15] LSND Collaboration, C. Athanassopoulos *et al.*, Phys. Rev. Lett. **77**, 3082 (1996); **81**, 1774 (1998); see also the LSND Collaboration home page at URL http://www.neutrino.lanl.gov/LSND/; KARMEN Collaboration, Phys. Rev. Lett. **81**, 520 (1998); Nucl. Phys. B (Proc. Suppl.) **77**, 212 (1999); see also the KARMEN Collaboration home page at URL http://www-ik1.fzk.de/www/karmen/karmen_e.html

[16] The MINOS Collaboration home page at URL http://www-numi.fnal.gov:8875/

[17] ICARUS Collaboration, F. Arneodo *et al.*, hep-ex/9812006; hep-ex/0103008; see also the ICARUS Collaboration home page at URL http://www.aquila.infn.it/icarus/

[18] A. Rubbia, Nucl. Phys. B (Proc. Suppl.) **91**, 223 (2000); see also the OPERA Collaboration home page at URL http://operaweb.web.cern.ch/operaweb/index.shtml

[19] The JHF Neutrino Working Group, Y. Itow *et al.*, hep-ex/0106019; see also the JHF Neutrino Working Group home page at URL http://neutrino.kek.jp/jhfnu/

[20] A. Bazarko *et al.*, Nucl. Phys. B (Proc. Suppl.) **91**, 210 (2000); hep-ex/0009056; see also the MiniBooNe Collaboration home page at URL http://www-boone.fnal.gov/

[21] See e.g., H. Minakata and H. Nunokawa, Phys. Rev. D **57**, 4403 (1998); Phys. Lett. B **413**, 369 (1997); **495**, 369 (2000); Nucl. Instrum. Methods Phys. Res. A **A472**, 421 (2000); J. High Energy Phys. **10**, 001 (2001); hep-ph/0111130; M. Koike and J. Sato, Phys. Rev. D **62**, 073006 (2000); J. Sato, Nucl. Instrum. Methods Phys. Res. A **451**, 36 (2000); K. Dick, M. Freund, P. Huber, and M. Lindner, Nucl. Phys. **B588**, 101 (2000); **B598**, 543 (2001); B. Richter, hep-ph/0008222; V. Barger, S. Geer, R. Raja, and K. Whisnant, Phys. Rev. D **63**, 113011 (2001); V. Barger *et al.*, hep-ph/0103052; L. Wai and B. Patterson, hep-ph/0101090; J. J. Gomez-Cadenas *et al.*, hep-ph/0105297; Zhi-zhong Xing, Phys. Rev. D **64**, 073014 (2001); Lian-You Shan, Bing-Lin Young, and Xinmin Zhang, *ibid.* **66**, 053012 (2002).

[22] See the J-PARC home page at URL http://j-parc.jp/

[23] S. Geer, Phys. Rev. D **57**, 6989 (1998); **59**, 039903(E) (1999); V. Barger, S. Geer, and K. Whisnant, *ibid.* **61**, 053004 (2000); V. Barger, S. Geer, R. Raja, and K. Whisnant, *ibid.* **62**, 013004 (2000); **62**, 073002 (2000); Phys. Lett. B **485**, 379 (2000); Phys. Rev. D **63**, 033002 (2001); S. Geer, Comments Nucl. Part. Phys. **A2**, 284 (2002).

[24] C. Albright *et al.*, hep-ex/0008064; M. L. Mangano *et al.*, hep-ph/0105155; J. Aysto *et al.*, hep-ph/0109217; A. De Roeck, J. Ellis, and F. Gianotti, hep-ex/0112004; T. Ota, J. Sato, and Y. Kuno, Phys. Lett. B **520**, 289 (2001).

[25] See, e.g., talk giving by Y. Kuno, at ''International Workshop on Nuclear and Particle Physics at 50-GeV PS,'' KEK, Japan, 2001, http://www-jhf.kek.jp/NP01/

[26] A part of this work has been reported by N. Okamura at BCP4, Ise, Japan, 2001; M. Aoki, K. Hagiwara, Y. Hayato, T. Kobayashi, T. Nakaya, K. Nishikawa, and N. Okamura, hep-ph/0104220.

[27] H. Chen *et al.*, hep-ph/0104266; Y. F. Wang *et al.*, Phys. Rev. D **65**, 073021 (2002).

[28] N. Cabibbo, Phys. Rev. Lett. **10**, 531 (1963); M. Kobayashi and T. Maskawa, Prog. Theor. Phys. **49**, 652 (1973).

[29] K. Hagiwara and N. Okamura, Nucl. Phys. **B548**, 60 (1999).

[30] C. Jarlskog, Phys. Rev. Lett. **55**, 1039 (1985); Z. Phys. C **29**, 491 (1985).

[31] See e.g., talk giving by M. Messier, at ''The 3rd Workshop on Neutrino Oscillations and their Origin (NOON2001),'' ICRR, Univ. of Tokyo, Kashiwa, Japan, Dec. 5–8, 2001, http://www-sk.icrr.u-tokyo.ac.jp/noon2001/

[32] H. Minakata, Phys. Lett. B **356**, 61 (1995); hep-ph/9612259; O. Yasuda and H. Minakata, hep-ph/9602386; O. Yasuda,

Phys. Rev. D **58**, 091301 (1998); G. L. Fogli, E. Lisi, D. Montanino, and A. Palazzo, *ibid.* **61**, 073009 (2000); G. L. Fogli, E. Lisi, A. Marrone, D. Montanio, and A. Palazzo, hep-ph/0104221; John N. Bahcall, M. C. Gonzalez-Garcia, and C. Pena-Garay, J. High Energy Phys. **04**, 007 (2002); M. C. Gonzalez-Garcia, M. Maltoni, C. Pena-Garay, and J. W. F. Valle, Phys. Rev. D **63**, 033005 (2001).

[33] C. Lunardini and A. Yu. Smirnov, Phys. Rev. D **63**, 073009 (2001); H. Minakata and H. Nunokawa, Phys. Lett. B **504**, 301 (2001).

[34] V. Barger, D. Marfatia, and B. P. Wood, Phys. Lett. B **532**, 19 (2002).

[35] See e.g., P. H. Frampton and S. L. Glashow, Phys. Lett. B **461**, 95 (1999); L. Hall, H. Murayama, and N. Weiner, Phys. Rev. Lett. **84**, 2572 (2000); E. Kh. Akhmedov, G. C. Branco, and M. N. Rebelo, Phys. Lett. B **478**, 215 (2000); D. Black, A. H. Fariborz, S. Nasri, and J. Schechter, Phys. Rev. D **62**, 073015 (2000); N. Haba, Y. Matsui, N. Okamura, and T. Suzuki, Phys. Lett. B **489**, 184 (2000); T. Miura, T. Shindou, E. Takasugi, and M. Yoshimura, Phys. Rev. D **63**, 053006 (2001); L. Lavoura, *ibid.* **62**, 093011 (2000); B. Stech, *ibid.* **62**, 093019 (2000); Y. Koide and A. Ghosal, Phys. Lett. B **488**, 344 (2000); N. Okamura and M. Tanimoto, Prog. Theor. Phys. **105**, 459 (2001); T. Miura, E. Takasugi, and M. Yoshimura, *ibid.* **104**, 1173 (2000); H. B. Nielsen and Y. Takanishi, Nucl. Phys. **B604**, 281 (2001); C. H. Albright and S. M. Barr, Phys. Rev. D **64**, 073010 (2001); H. Fritzsch and Z. Z. Xing, Phys. Lett. B **517**, 363 (2001).

[36] A. M. Dziewonski and D. L. Anderson, Phys. Earth Planet. Inter. **25**, 297 (1981).

[37] See e.g., J. Arafune, M. Koike, and J. Sato, Phys. Rev. D **56**, 3093 (1997); **60**, 119905(E) (1999); M. Koike and J. Sato, Mod. Phys. Lett. A **14**, 1297 (1999); T. Ota and J. Sato, Phys. Rev. D **63**, 093004 (2001); T. Miura, T. Shindou, E. Takasugi, and M. Yoshimura, *ibid.* **64**, 013002 (2001); **64**, 073017 (2001).

[38] Y. Yamanoi *et al.*, ''Large Horn Magnets at the KEK Neutrino Beam Line,'' KEK Report No. 97-225, November, 1997.

[39] D. Beavis *et al.*, BNL E-889 proposal.

[40] T. Kobayashi for the JHF Neutrino Working Group, talk given at the Fifth KEK Topical Conference, KEK, Tsukuba, Japan, November, 2001.

[41] R. Brun and F. Carminati, ''GEANT Detector Description and Simulation Tool,'' CERN Program Library Long Write-up W5013, September, 1993.

[42] C. Zeitnitz and T. A. Gabriel, Nucl. Instrum. Methods Phys. Res. A **349**, 106 (1994); T. A. Gabriel, J. D. Amburgey, and B. L. Bishop, ''Calor: A Monte Carlo Program Package For The Design And Analysis Of Calorimeter Systems,'' Report No. ORNL/TM-5619; C. Zeitnitz and T. A. Gabriel, Nucl. Instrum. Methods Phys. Res. A **349**, 106 (1994).

[43] See the home page at URL http://neutrino.kek.jp/JHF-VLBL/flux/

[44] See e.g., K. Ishihara, Ph.D. thesis, ICRR Report No. 457-2000-1; Y. Hayato, talk at NuInt01, KEK, December 13–16, to appear in the proceedings.

[45] Particle Data Group, D. Groom *et al.*, Eur. Phys. J. C **15**, 1 (2000).

[46] See the home page of the Borexino Collaboration at URL http://almime.mi.infn.it/

[47] See the KamLAND Collaboration home page at URL http://www.awa.tohoku.ac.jp/html/KamLAND/index.html

[48] V. Barger, D. Marfatia, and B. P. Wood, Phys. Lett. B **498**, 53 (2001); A. Gouvêa and C. Pene-Garay, Phys. Rev. D **64**, 113011 (2001); A. Strumia and F. Vissani, J. High Energy Phys. **11**, 048 (2001).

[49] M. Aoki, K. Hagiwara, and N. Okamura, Phys. Lett. B **554**, 121 (2003).

[50] C. K. Jung for the K2K Collaboration, talk given at XX International Symposium on Lepton and Photon Interactions at High Energies, Rome, Italy, 2001.

[51] The KamLAND Collaboration, K. Eguchi *et al.*, Phys. Rev. Lett. **90**, 021802 (2003).